

How do Cl concentrations matter for simulating CH₄, δ¹³C(CH₄) and estimating CH₄ budget through atmospheric inversions ?

Joël Thanwerdas^{1,*}, Marielle Saunois¹, Isabelle Pison¹, Didier Hauglustaine¹, Antoine Berchet¹, Bianca Baier^{2,3}, Colm Sweeney³, and Philippe Bousquet¹

¹Laboratoire des Sciences du Climat et de l'Environnement, LSCE-IPSL (CEA-CNRS-UVSQ), Université Paris-Saclay 91191 Gif-sur-Yvette, France.

²Cooperative Institute for Research in Environmental Sciences (CIRES), University of Colorado-Boulder, Boulder, CO, USA 80305.

³NOAA Earth System Research Laboratory Global Monitoring Division, Boulder, CO, USA 80305.

Correspondence: J. Thanwerdas (joel.thanwerdas@lscce.ipsl.fr)

Abstract. Atmospheric methane (CH₄) concentrations have been rising since 2007, ~~resulting from due to~~ an imbalance between CH₄ sources and sinks. The CH₄ budget is generally estimated through top-down approaches using chemistry-transport models (CTMs) and CH₄ observations as constraints. The atmospheric isotopic CH₄ signal composition, δ¹³C(CH₄), can also provide additional constraints and helps to discriminate between emission categories. Nevertheless, to be able to use the
5 information contained in these observations, the models must correctly account for processes influencing δ¹³C(CH₄). The oxidation by chlorine (Cl) likely contributes less than 5% to the total oxidation of atmospheric CH₄. However, the Cl sink is highly fractionating large kinetic isotope effect of the Cl sink kinetics produces a large fractionation of ¹³C compared with ¹²C in atmospheric methane, and thus strongly influences δ¹³C(CH₄). ~~As inversion studies~~ When integrating the Cl sink in their setup to constrain the CH₄ budget, which is not yet standard, atmospheric inversion
10 do not prescribe the same Cl fields~~to constrain budget, it can lead, therefore leading~~ to discrepancies between flux estimates. To quantify the influence of the Cl concentrations on CH₄, δ¹³C(CH₄) and CH₄ budget estimates, we perform multiple sensitivity simulations using ~~three Cl fields with concentrations that are realistic with regard to recent literature and one Cl field with concentrations that are very likely to be overestimated~~ four different Cl fields. We also test removing the tropospheric and the entire Cl sink ~~in other sensitivity simulations.~~ We find that the ~~realistic~~ Cl fields tested here are responsible for between 0.3% and 1.8% and 8.5% of
15 the total chemical CH₄ sink in the troposphere and between 1.0% and 1.2% and 1.6% in the stratosphere. Prescribing these different Cl amounts in ~~surface-based atmospheric~~ inversions can lead to differences of up to 53.8 TgCH₄.yr⁻¹ in global CH₄ source adjustments emissions and of up to 12.3. ~~We also find that 4.7‰ in the globally-averaged isotopic signature of the total CH₄ sources inferred by a surface-based inversion assimilating observations would decrease by 0.53 source (δ¹³C(CH₄)_{source).}~~ More specifically, each increase by 1000 molec.cm⁻³ in the mean tropospheric Cl concentration would result in an adjustment
20 by +11.7 TgCH₄.yr⁻¹ for global CH₄ emissions and -1.0‰ for each additional percent of contribution from the tropospheric Cl sink to the total sink. Finally, our study shows that the globally-averaged δ¹³C(CH₄)_{source.} Our study also shows that if the CH₄ seasonal cycle amplitude is only modified by less than 1-2% but ‰, the δ¹³C(CH₄) seasonal cycle amplitude can be significantly modified by up to 10-20%, depending on the latitude. In an atmospheric inversion performed with isotopic

constraints, this influence can result in significant differences in the posterior source mixture. For example, the contribution from wetlands emissions to total emissions can be modified by about 0.8 % to adjust the globally-averaged $\delta^{13}\text{C}(\text{CH}_4)_{\text{source}}$, corresponding to a $15 \text{ TgCH}_4 \cdot \text{yr}^{-1}$ change. Finally, tested Cl concentrations have a large influence on the simulated $\delta^{13}\text{C}(\text{CH}_4)$ vertical profiles above 30 km, albeit this influence is small below this altitude, and they have a very small influence on the simulated CH_4 vertical profiles. Overall, our model captures well the observed CH_4 and $\delta^{13}\text{C}(\text{CH}_4)$ vertical profiles, especially in the troposphere and it is difficult to prefer one Cl field over another based uniquely on the available observations of vertical profiles.

1 Introduction

Methane (CH_4) is a very important species for both atmospheric chemistry and climate. Its atmospheric mole fractions have reached an average of $1879\text{--}1896$ ppb at the surface in ~~2020 (Dlugokencky, 2021)~~ 2021 (Dlugokencky, 2022), almost three times higher than pre-industrial mole fractions (Etheridge et al., 1998). After a plateau between 1999 and 2006, CH_4 mole fractions resumed their increase in 2007 without showing any sign of stabilization since then. The increase has even reached an unprecedented value of $+15.9\text{--}16.9$ ppb for the year ~~2020–2021 (Dlugokencky, 2022)~~. The accumulation of CH_4 (~ 8 ppb $\cdot\text{yr}^{-1}$ on average since 2007) in the atmosphere is the result of ~~a slight imbalance~~ an imbalance of about $20 \text{ TgCH}_4 \cdot \text{yr}^{-1}$ (Saunio et al., 2020) between sources that release CH_4 into the atmosphere and sinks that remove it. Sinks are mostly due to oxidation reactions in the atmosphere ~~–Three radicals react with~~ between CH_4 ~~in the atmosphere~~ and three radicals: hydroxyl (OH), atomic oxygen (O^1D), and chlorine (Cl). These chemical reactions account for about 93 % of the total CH_4 sink, with the remainder being removed by methanotrophic bacteria in the soil (Saunio et al., 2020). On the other hand, CH_4 sources are varied and result from radically different processes (biogenic, thermogenic and pyrogenic).

Estimating global CH_4 sources with precision is a mandatory step, yet challenging, towards implementing efficient mitigation policies. Top-down atmospheric inversions are known to be efficient approaches to estimate CH_4 sources at different scales and have become increasingly relevant over the years as observational networks have developed (Houweling et al., 2017, and references therein). However, inversions that assimilate only total CH_4 observations can only rely on variations in seasonal cycles to differentiate co-located emissions. To better separate these sources, assimilating observations of the $^{13}\text{C}:^{12}\text{C}$ atmospheric isotope signal composition of CH_4 , denoted by $\delta^{13}\text{C}(\text{CH}_4)$, can be relevant. This value is based on the ratio between the isotopologue $^{12}\text{CH}_4$, which represents about 99 % of the CH_4 in the atmosphere (Stolper et al., 2014) and its counterpart $^{13}\text{CH}_4$. $\delta^{13}\text{C}(\text{CH}_4)$ is commonly defined using a deviation of the sample mole-atomic isotopic ratio relative to a specific standard ratio :

$$\delta^{13}\text{C}(\text{CH}_4) = \frac{R}{R_{\text{std}}} - 1 = \frac{[^{13}\text{CH}_4]/[^{12}\text{CH}_4]}{R_{\text{std}}} - 1 \quad (1)$$

~~and denote the and mole fractions, respectively~~ R represents the abundance of ^{13}C relative to ^{12}C in all CH_4 molecules. $R_{\text{std}} = 0.0112372$ is here the standard ratio of Vienna - Pee Dee Belemnite (PDB VPDB) (Craig, 1957).

55 CH₄ sources exhibit specific isotopic signatures that are mainly controlled by the process involved in the production of CH₄. Broadly summarized, most biogenic sources have an isotopic signature between -65 and -55 ‰, thermogenic sources between -50 and -30 ‰ and pyrogenic sources between -25 ‰ and -15 ‰ (Sherwood et al., 2017), although the ~~distributions~~ full distributions of these signatures are very large ~~and overlaps exist between the extreme~~ with overlapping values. The post-2007 CH₄ increase is notably associated with a decrease in the atmospheric isotopic signal composition $\delta^{13}\text{C}(\text{CH}_4)$ (Nisbet et al., 60 2019) ~~and these isotopic variations that~~ could help to better explain ~~this renewed growth and the renewed~~ CH₄ growth and, more specifically, the contribution from the different CH₄ sources to it.

The sinks ~~are also fractionating,~~ also have an influence on $\delta^{13}\text{C}(\text{CH}_4)$ as they remove ¹²CH₄ faster than ¹³CH₄. This effect, called the Kinetic Isotope Effect (KIE) or isotopic fractionation, is quantified using the ratio of the reaction rate constants $X + ^{12}\text{CH}_4$ and $X + ^{13}\text{CH}_4$, with X the species of interest ($X = \text{OH}, \text{O}(^1\text{D})$ or Cl). $\text{KIE}_X = k_{12}^X/k_{13}^X$ with k_{12}^X and k_{13}^X being the 65 oxidation reaction rate constants. As a result, $\delta^{13}\text{C}(\text{CH}_4)$ depends on both sources and sinks, as-like total CH₄, but also on the isotopic fractionation and the ~~sources isotopic signatures~~ isotopic signatures of the sources.

Among all CH₄ sinks, the Cl sink accounts for a small part of the total CH₄ oxidation. Following the discovery of the dramatic impact of Cl on ozone in the stratosphere, many studies have ~~first~~ focused on the impact of stratospheric Cl on CH₄ and $\delta^{13}\text{C}(\text{CH}_4)$ using box or 2-D models (e.g., Röckmann et al., 2004; McCarthy et al., 2003; Wang et al., 2002; McCarthy 70 et al., 2001; Saueressig et al., 2001; Gupta et al., 1996; Müller et al., 1996). McCarthy et al. (2003) estimated that Cl was responsible for 20-35 % of CH₄ removal in the stratosphere. Saunio et al. (2020) suggested a range of values for the total stratospheric sink between 12 and 37 TgCH₄.yr⁻¹, leading to a plausible stratospheric Cl sink of 2-13 TgCH₄.yr⁻¹, or about only 0.4-2.4 % of the total CH₄ oxidation in the atmosphere. Although this contribution is very small, the Cl sink is particularly important because of its large fractionation effect (KIE = 1.066 for the Cl sink against 1.0039 for the OH sink, see Sect. 2.1). 75 The aforementioned studies showed that stratospheric Cl has a strong impact on $\delta^{13}\text{C}(\text{CH}_4)$ not only in the stratosphere but also at closer to the surface. In particular, Wang et al. (2002) estimated that stratospheric Cl was responsible for a $\delta^{13}\text{C}(\text{CH}_4)$ enhancement of 0.23 ‰ at the surface between 1970 and 1992 due to stratosphere-troposphere exchanges (STE).

In the troposphere, the Cl sink likely accounts for less than 5 % of CH₄ oxidation (Wang et al., 2019, 2021; Hossaini et al., 2016; Sherwen et al., 2016b; Gromov et al., 2018; Allan et al., 2007). Several studies have estimated Cl concentrations in the 80 troposphere and in the Marine Boundary Layer (MBL) and discussed the Cl sink. Allan et al. (2007) estimated the Cl sink in the troposphere to be 25 TgCH₄.yr⁻¹, representing about 5 % of the total CH₄ chemical sink. More recently, Hossaini et al. (2016), Sherwen et al. (2016b), Wang et al. (2019) and Wang et al. (2021) have made important developments in tropospheric chemistry modeling (see Sect 2.2) and obtained oxidation contributions of 2.6 %, 2 %, 1 % and 0.8 % respectively with mean tropospheric Cl concentrations between 620 and 1300 molec.cm⁻³. However, Gromov et al. (2018) concluded that variations 85 in Cl concentrations above 900 molec.cm⁻³ in the extratropical part of the Southern Hemisphere are very unlikely ; thus suggesting that the high estimates from Allan et al. (2007) and Hossaini et al. (2016) are likely overestimated. ~~These variations~~ in This estimated range of oxidation contributions may appear small but Strode et al. (2020) recently showed a high sensitivity of the tropospheric $\delta^{13}\text{C}(\text{CH}_4)$ distribution to variation in Cl fields by testing, among others, those of Allan et al. (2007), Sherwen et al. (2016b) and Hossaini et al. (2016), indicating that each percent increase in how much CH₄ is oxidized by Cl

90 leads to a 0.5 ‰ increase in $\delta^{13}\text{C}(\text{CH}_4)$, therefore larger than the global downward shift observed since 2007 (Nisbet et al., 2019).

Forward and inverse 3-D modeling studies focusing on CH_4 and $\delta^{13}\text{C}(\text{CH}_4)$ consider the Cl sink at different level of ~~details~~detail. Most studies consider only the Cl sink in the stratosphere (e.g., Fujita et al., 2020; Rigby et al., 2012; Monteil et al., 2011; Fletcher et al., 2004), and a very few account for tropospheric Cl only (e.g., Thompson et al., 2018). In single-box
95 models, sinks are combined and an overall fractionation coefficient is used (e.g., Schaefer et al., 2016; Schwietzke et al., 2016). In recent studies, Cl is often prescribed in both the troposphere and stratosphere (e.g., McNorton et al., 2018; Rice et al., 2016; Warwick et al., 2016; Neef et al., 2010), although most studies use the Cl ~~configuration~~distribution suggested by Allan et al. (2007), which is likely to be overestimated as mentioned above.

In the atmospheric inversions performed with the LMDz-SACS chemistry-transport model (Locatelli et al., 2015; Pison
100 et al., 2009), the Cl sink was omitted so far, even in the stratosphere (Saunio et al., 2020; Locatelli et al., 2015; Pison et al., 2009; Bousquet et al., 2006). For these studies assimilating only total CH_4 observations, the impact of the Cl sink on the estimated CH_4 emissions was considered negligible. However, the number and quality of isotopic observations have considerably increased since the 2000s, and developments of the CIF-LMDz-SACS inversion system to use the isotopic constraint have been made (Thanwerdas et al., 2021). Joint assimilation (CH_4 and $\delta^{13}\text{C}(\text{CH}_4)$) is proving to be relevant and necessary in order
105 to reconcile the estimated CH_4 budgets with the atmospheric isotope signalcomposition. Considering the large impact of the Cl sink on $\delta^{13}\text{C}(\text{CH}_4)$, it is necessary to include and evaluate the Cl sink and its impact on the simulation of CH_4 modeling processand $\delta^{13}\text{C}(\text{CH}_4)$ with our model.

Here, we detail the influence of tropospheric and stratospheric Cl on the modeling of CH_4 and $\delta^{13}\text{C}(\text{CH}_4)$ in LMDz-SACS by using several Cl fields. ~~Ultimate goal being to use the isotopic signal~~The ultimate aim is to assimilate the isotopic
110 composition observations to perform multi-constraint inversions with the LMDz-SACS model; ~~results are analyzed throughout the study under~~. Therefore the developments performed and the results obtained are analyzed through the prism of atmospheric inversion. In ~~the first part~~Sect. 2, we present the characteristics of the available Cl fields, model inputs and observations used for evaluation. ~~Then~~In Sect. 3, we analyze the influence of the different Cl fields on CH_4 and $\delta^{13}\text{C}(\text{CH}_4)$ at the surface, on global CH_4 flux and $\delta^{13}\text{C}(\text{CH}_4)$ source signature adjustment obtained with inversion methods and on the CH_4 ~~vertical profile~~and
115 $\delta^{13}\text{C}(\text{CH}_4)$ vertical profiles.

2 Methods

2.1 The chemistry-transport model (CTM)

The general circulation model (GCM) LMDz is the atmospheric component of the coupled model of the Institut Pierre-Simon Laplace (IPSL-CM) developed at the Laboratoire de Météorologie Dynamique (LMD) (Hourdin et al., 2006). The version
120 of LMDz used here is an "offline" version dedicated to the inversion framework created by Chevallier et al. (2005): the pre-calculated meteorological fields provided by the online version of LMDz are given as input to the model, which considerably reduces the computation time. The model is built at a horizontal resolution of $3.8^\circ \times 1.9^\circ$ (96 grid cells in longitude and latitude)

with 39 hybrid sigma pressure levels reaching an altitude of about 75 km. About 20 levels are ~~dedicated to~~ located in the stratosphere and ~~the mesosphere~~ above. The time step of the model is 30 min and the output values have a resolution of 3 hours.

125 Horizontal winds have been nudged towards the ECMWF meteorological analyses (ERA-Interim) in the online version of the model. Vertical diffusion is parameterised by a local approach of Louis (1979), and deep convection processes are parameterised by the scheme of Tiedtke (1989). The offline model LMDz, coupled with the Simplified Atmospheric Chemistry System (SACS) module (Pison et al., 2009), was previously used to simulate atmospheric mole fractions of trace gases such as CH₄, carbon monoxide (CO), methyl chloroform (MCF), formaldehyde (CH₂O) or hydrogen (H₂). This system has been recently

130 converted into a chemistry parsing system (Thanwerdas et al., 2021). It follows the principle of the chemical parsing system of the regional model CHIMERE (Mailler et al., 2017; Menut et al., 2013) and allows the user to prescribe the set of chemical reactions to consider. Consequently, it generalizes the SACS module to any set of possible reactions. The concentration fields of the different species are either prescribed or simulated. Prescribed species (here OH, O(¹D) and Cl) are not transported in LMDz, and their mole fractions are not updated by chemical production or destruction. These species are only used to

135 calculate reaction rates and update the mole fractions of transported species at each iteration of the model. In this study, the ¹²CH₄ and ¹³CH₄ isotopologues are simulated as separate tracers and CH₄ mole fractions are defined as ~~a sum of~~ the sum of the mole fractions of the two isotopologues. Oxidation by Cl + CH₄ was added to complete the chemical removal of CH₄, which only considered OH + CH₄ and O(¹D) + CH₄ reactions in the original SACS chemical scheme. The photolysis of CH₄ is not included in SACS as it is considered negligible. None of the inversion studies mentioned above, in particular those of

140 Saunois et al. (2020), accounted for this sink.

Reactions between ¹²CH₄ and OH, O(¹D) and Cl are represented by the chemical equations below, and similar equations apply to ¹³CH₄ :



Three-dimensional and time-dependent oxidant concentration fields (OH, O(¹D) and Cl) were simulated by the GCM LMDz coupled to the INteraction with Chemistry and Aerosols (INCA) model (Hauglustaine et al., 2021; Folberth et al., 2006; Hauglustaine et al., 2004). Seventeen ozone-depleting substances ~~consisted~~ consisting of CFCs (CFC-12, CFC-11, CFC-113),

150 three HCFCs (HCFC-22, HCFC-141b, HCFC-142b), two halons (Halon-1211, Halon-1301), methyl chloroform (CH₃CCl₃ or MCF), carbon tetrachloride (CCl₄), methylchloride (CH₃Cl), methylene chloride (CH₂Cl₂), chloroform (CHCl₃), methyl bromide (CH₃Br) and HFC-134a, and their associated photochemical reactions, were included in the INCA chemical scheme to produce Cl radicals (~~?)~~ (Terrenoire et al., 2022). In the LMDz-INCA simulations, surface concentrations of these long-lived Cl ~~source species~~ precursors were prescribed based on historical data sets prepared by Meinshausen et al. (2017). The model

155 was run for the 1850-2018 period (Hauglustaine et al., 2021).

Table 1. Reaction rate constants and KIEs of CH₄ chemical sinks. The reaction rate constants are taken from Burkholder et al. (2015).

Oxidant	KIE	Reference	Reaction rate constant (cm ³ molec ⁻¹ s ⁻¹)
OH	1.0039	Saueressig et al. (2001)	$2.45 \times 10^{-12} \cdot \exp(-1775/T)$
Cl	$1.043 \cdot \exp(6.455/T)$	Saueressig et al. (1995)	$7.1 \times 10^{-12} \cdot \exp(-1280/T)$
O(¹ D) - R3	1.013	Saueressig et al. (2001)	1.125×10^{-10}
O(¹ D) - R4	1.013	Saueressig et al. (2001)	3.75×10^{-11}

All reaction rate constants and associated values [used in LMDz-SACS](#) are given in Table 1. The reaction rate constants with ¹³CH₄ are modified based on the definition of the [fractionation coefficient \(KIE\)](#)~~KIE~~. Few studies have evaluated the KIEs associated with CH₄ chemical sinks (particularly for O(¹D) and Cl) over a wide range of temperatures and thus large uncertainties remain. For CH₄ + OH, we adopted the value of Saueressig et al. (2001) as they indicate that this data is of considerably higher experimental precision and reproducibility than previous studies, in particular Cantrell et al. (1990), which suggested a value of 1.0054.

2.2 Description of Cl fields

Four fields of Cl are ~~used compared~~ in this study. ~~The first field was simulated by the~~ [Two fields were generously provided by the respective authors of Sherwen et al. \(2016b\) and Wang et al. \(2021\). They will be referred to as the Cl-Sherwen and Cl-Wang fields. Sherwen et al. \(2016b\) obtained the associated Cl field using version 10 of the GEOS-Chem CTM \(<https://geos-chem.seas.harvard.edu/>, version 10\) running at a 4° × 5° spatial resolution. Previously, Sherwen et al. \(2016a\) extended the stratospheric chlorine scheme to the troposphere. Sherwen et al. \(2016b\) improved the coupling of halogens \(Br, Cl, I\) chemistry and further updated the chlorine chemistry scheme. Subsequently, Wang et al. \(2019\) focused principally on the modelling of tropospheric reactive chlorine by developing the treatment of sea salt aerosol \(SSA\) chloride and chlorine gases, as well as SSA acid displacement thermodynamics, starting from version 11-02d of GEOS-Chem. Chloride mobilisation from SSA by acid displacement of HCl represents a significant source of reactive chlorine in the troposphere. The authors also mentioned a better accounting of other chlorine sources \(combustion, organochlorines, transport from the stratosphere, anthropogenic HCl\) compared to previous versions. Wang et al. \(2020, 2021\) made some additional developments that appear to have a relatively small impact on the atomic Cl spatial distribution and mean concentration in the troposphere. They did not include continental anthropogenic emissions of inorganic Cl \(coal combustion, waste incineration, and industrial activities\) because existing estimates are likely outdated and carry too high uncertainties. Consequently, the Cl concentrations from Wang et al. \(2021\) may be underestimated over regions where relatively high anthropogenic chlorine sources have been reported \(e.g. China\).](#)

~~Another field was simulated by the LMDz-INCA model, as mentioned above. More details on the modeling of this field are available in the supplement model, as mentioned in Sect. 2.1.~~ This field will be referred to as the Cl-INCA field. At ~~this stage~~[present](#), simulations performed with the LMDz-INCA model do not fully represent the chemical interactions between

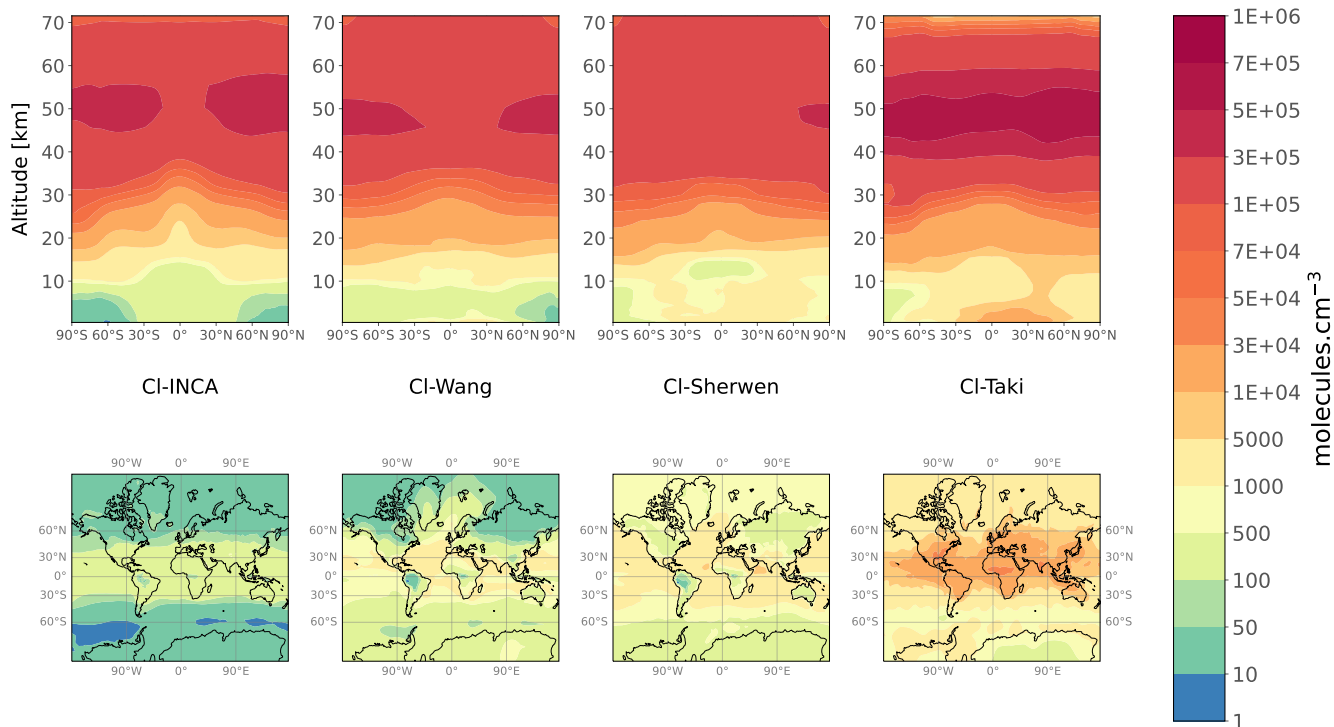


Figure 1. Annual mean meridional cross-section (upper panels) and tropospheric Cl concentrations (lower panels) for the four 3-D fields CI-INCA, CI-Wang, CI-Sherwen and CI-Taki.

Cl and other species in the troposphere. ~~Developments In particular, developments~~ are currently being made to improve ~~these interactions~~ the treatment of SSA and chloride mobilisation from SSA. CI-INCA did not benefit from such enhancements, resulting in significant discrepancies compared to CI-Wang and CI-Sherwen. The mean tropospheric Cl concentration ($330 \text{ molec.cm}^{-3}$) in the CI-INCA field is ~~therefore about half lower than the mean tropospheric value about half of the tropospheric mean~~ ($630 \text{ molec.cm}^{-3}$) of Wang et al. (2021) ~~or other studies, but, but is~~ in agreement with the upper limits inferred by Gromov et al. (2018).

Two fields were simulated using the versions of the GEOS-Chem model (v10 and v12.9, respectively) of Sherwen et al. (2016b) and Wang et al. (2021) (i.e., v10 and v12.9, respectively). These fields were generously provided by the respective authors of the two studies. They will be referred to as the CI-Sherwen and CI-Wang fields. Differences between the two fields are detailed below.

The last field was simulated by version 5.7b of the CCSR/NIES/FRCGC (Center for Climate System Research/National Institute for Environmental Studies/Frontier Research Center for Global Change) atmospheric GCM (Takigawa et al., 1999). This was provided by the GCP-GMB (Global Carbon Project - Global Methane Budget) team to run the inversions used in Saunio et al. (2020), although it was not mandatory. It is referred to as the CI-Taki field.

Annual mean meridional cross-section (upper panels) and tropospheric Cl concentrations (lower panels) for the four 3-D fields CI-INCA, CI-Wang, CI-Sherwen and CI-Taki.

In this study, we do not test the Cl fields from Hossaini et al. (2016) and Allan et al. (2007) because we want to carry out the sensitivity analysis while keeping a realistic and up-to-date range of concentrations. Their concentrations are indeed very likely to be overestimated (Gromov et al., 2018). Although Cl concentrations in the some inversions did not prescribe it. The model did not include any treatment of SSA and chloride mobilisation from SSA. More generally, it did not include any representation of tropospheric reactive chlorine chemistry. We could not have access to additional information regarding this field. It is referred to as the Cl-Taki field are also very large, to our knowledge, oxidation resulting from the prescription of this field has not been studied before. We therefore choose to include it here in order to quantify the associated sink and to illustrate the influence of such concentrations on and field.

The four fields are shown in Fig. 1. We use the lapse rate (2 K/km) definition from the World Meteorological Organization (WMO) and the meteorological fields from the online LMDz model to define the tropopause. Global mean tropospheric Cl concentrations range ~~between from~~ 330 (Cl-INCA) ~~and to~~ 4730 (Cl-Taki) molec.cm⁻³. The latitudinal distributions of tropospheric concentrations are similar, although Cl-Wang, Cl-Sherwen and Cl-Taki have a greater spatial variability around their mean value than Cl-INCA, especially in the mid-latitudes (75 %, 66 % and 63 % against 36 %, respectively). Cl-Wang, Cl-Sherwen and Cl-INCA ~~exhibits~~ exhibit similar concentrations in the stratosphere ($1.45 \pm 0.07 \times 10^5$ molec.cm⁻³). The increase in concentrations with altitude between the surface and 30 km is similar between all ~~the~~ fields, with a 0-30 km vertical gradient of $4.4 \pm 1.0 \times 10^4$ molec.cm⁻³. Stratospheric concentrations are however larger in Cl-Taki, reaching a mean value of 2.1×10^5 molec.cm⁻³.

In this study, we do not test the Cl fields from Hossaini et al. (2016) and Allan et al. (2007) because the fields presented above cover a range of tropospheric and stratospheric Cl concentrations wide enough to carry out a robust analysis.

2.3 Description of simulations

The time period adopted for all simulations here is 1998-2018, long enough to capture the large equilibration time associated with $\delta^{13}\text{C}(\text{CH}_4)$. Mole fractions of $^{12}\text{CH}_4$ and $^{13}\text{CH}_4$ are simulated over the 1998-2018 period. The distributions of OH and O(¹D) have also been simulated with the LMDz-INCA model and are outputs of the same simulation that provided the Cl-INCA field. These OH and O(¹D) fields are used in all simulations performed here this period of time in multiple simulations, either forward or inverse.

~~Our SimREF reference simulation uses the Cl-Wang field as it is the most recent field and is taken from the most comprehensive study to date. In addition, we want our reference simulation to infer realistic and distributions with a good model-observation agreement. The fluxes and isotopic signatures of five emission categories used in this study therefore result from an atmospheric inversion. First, a set of optimized fluxes and source signatures are obtained by running atmospheric variational inversions over 1998-2018 based on a joint assimilation of CH_4 and $\delta^{13}\text{C}(\text{CH}_4)$ in the CIF-LMDz-SACS system designed by Thanwerdas et al. (2021). The inversion assimilates observations introduced in Sect. 2.4. The Cl-Wang field was not available when this inversion was launched. Therefore, we instead prescribed the Cl-INCA field and scaled the tropospheric mean Cl concentration (330) to that of Wang et al. (2019) (620), very similar to that of Wang et al. (2021) (630). We acknowledge the small difference between the inversion setup and the reference scenario setup, due to small differences in Cl concentrations. However, using the~~

235 ~~optimized fluxes and signatures together with the prescribed sinks, a model-observation agreement (Root Mean Square Error) of 3.6 ppb for~~ A variational inversion consists in performing alternate runs of the CTM's forward and adjoint codes to calculate the cost function and its gradient. A global minimum of this cost function is then sought using an adequate minimization algorithm. With our method, multiple iterations of this process are performed until a satisfactory convergence criterium is reached. At the end of the minimization process, we obtain posterior fluxes and source signatures that reduce the discrepancies between observed and simulated CH_4 and 0.04 for $\delta^{13}\text{C}(\text{CH}_4)$ ~~is obtained on global averages, and is considered sufficient to validate the conclusions of this study. More information about the inversion is given in the supplement (Text S1). Emissions and source isotopic signatures are given in Table ??.~~ Both vary over time and space and are prescribed as monthly fields at the horizontal resolution of the model.

240 ~~The~~, compared with prior estimates. Our system typically runs a last forward simulation with optimized inputs at the end of the inversion process.

One variational inversion is run for each CI field presented in Sect. 2.2. The CI-Wang, CI-Sherwen, CI-Taki and CI-INCA fields ~~presented in Sect. 2.2~~ are used in the ~~SimSherwen, SimTaki and SimINCA simulations~~ INV-Wang, INV-Sherwen, INV-Taki and INV-INCA inversions, respectively. In Saunio et al. (2020), the majority of inversions ~~are~~ were performed without a tropospheric CI sink; thus, we ~~tested this with the SimNoTropo simulation where~~ perform one inversion using the CI-Wang ~~is used but with no CI in the troposphere. Moreover~~ field but without tropospheric CI (INV-NoTropo). Finally, as LMDz-SACS completely omitted the CI sink in previous studies, we estimate the errors generated by this omission ~~running the SimNoCI simulation, which has no CI sink. A summary of the simulations and their characteristics is provided by~~ running a last inversion without CI sink (INV-NoCI). More information about the variational inversion method, the inversion system used here and the setup of these inversions is provided in the supplement (Text S1). Apart from the prescribed CI field, all these inversions share the same configuration. Consequently, for each inversion, we obtain a different set of fluxes and source signatures and the differences between them result only from the influence of CI concentrations. These differences are analyzed in Sect. 3.3 and Sect. 3.4.

255 As mentioned above, the last forward simulation of a variational inversion is performed with optimized inputs. Hereinafter, INV-* outputs (simulated values) refer to the results of the last forward simulation performed with the optimized fluxes and source signatures derived from the corresponding inversion, prescribed as monthly fields at the horizontal resolution of the model. As expected, CH_4 and $\delta^{13}\text{C}(\text{CH}_4)$ simulated with the posterior fluxes and source signatures are all consistent with assimilated observations (see supplementary Fig. S1). Emissions and source isotopic signatures obtained with INV-Wang are given in Table 32. They both vary over time and space.

260 A set of simple forward simulations (FWD-*) with identical prescribed fluxes and source signatures are also run to quantify the biases in CH_4 and $\delta^{13}\text{C}(\text{CH}_4)$ that arise from differences in prescribed CI field, hence differences in atmospheric sink. The posterior fluxes and source signatures from INV-Wang are used for all FWD-* simulations because the CI-Wang field is taken from the most comprehensive and recent study to date. A different CI field is prescribed for each simulation, resulting in six forward simulations : FWD-Wang, FWD-Sherwen, FWD-Taki, FWD-INCA, FWD-NoTropo and FWD-NoCI. Apart from the

265 prescribed Cl field, all these simulations adopt the same configuration. Consequently, note that the FWD-Wang and INV-Wang
inputs and outputs are identical.

To summarize :

- INV-* outputs are consistent with observed CH₄ and $\delta^{13}\text{C}(\text{CH}_4)$ because they use optimized fluxes and source signatures
derived from a variational inversion.
- 270 - Apart from FWD-Wang, FWD-* outputs are not consistent with observed values because they all adopt the same fluxes
and source signatures.

Table 2. Global CH₄ emissions and associated flux-weighted isotopic signatures by source category obtained with INV-Wang. Given values are averages over 1998-2018. Numbers in brackets are minimum and maximum over this period of time [min/max].

Categories	CH ₄ emissions (TgCH ₄ .yr ⁻¹)	Isotopic signature (‰ - VPDB)
Biofuels-Biomass Burning (BB)	28 [23 / 44]	-21.5 [-22.2 / -21.3]
Agriculture and Waste (AGW)	221 [197 / 241]	-58.3 [-59.4 / -57.0]
Fossil Fuels and Geological sources (FFG)	124 [101 / 142]	-43.5 [-44.8 / -42.1]
Natural sources apart from wetlands (NAT)	23 [23 / 23]	-50.8 [-50.8 / -50.8]
Wetlands (WET)	192 [184 / 202]	-56.6 [-56.6 / -56.5]
Total	588 [530 / 639]	-52.6 [-53.3 / -52.0]

2.4 Observations

Different datasets of observations are either assimilated in our inversions or used to evaluate our simulations and to estimate the impact of the Cl field. These observations are of several types ~~and could be assimilated in atmospheric inversions~~: surface
275 measurements of CH₄ and $\delta^{13}\text{C}(\text{CH}_4)$ ~~as well as~~ in situ vertical profiles of CH₄ ~~and in situ vertical profiles of $\delta^{13}\text{C}(\text{CH}_4)$~~

CH₄ observations measured at 79 surface stations of the Global Greenhouse Gas Reference Network (GGGRN), part of the NOAA-ESRL's Global Monitoring Laboratory (NOAA GML), ~~were used to perform the inversion~~ are assimilated in the
inversions introduced in Sect. ~~??2.3~~. Reported uncertainties are generally below 5 ppb. $\delta^{13}\text{C}(\text{CH}_4)$ measurements provided by the Institute of Arctic and Alpine Research (INSTAAR) by analyzing air samples collected at 22 stations on an approximately
280 weekly basis ~~were~~ are also assimilated (White et al., 2021). Reported uncertainties are generally below 0.15 ‰.

~~A total of 11 MBL sites (i.e., the site samples consist mainly of well-mixed MBL air) among those that recorded values over the 1998-2018 period were selected to sample simulated values at the time and locations of available observations.~~ The station locations and additional information can be found in the supplementary Figure S3, Tables ~~S5 and S6~~ and S7.

~~Finally, an~~

285 An analysis of the impact of Cl on CH₄ vertical profiles is also conducted using a set of 115 AirCore profiles recovered from 11 different sites over the 2012-2018 period. A total of 80 profiles are provided by the NOAA GML aircraft programme (Baier

Table 3. Nomenclature and description of the sensitivity tests [performed in this study](#). The INV-* simulations refer both to the variational inversion performed with the system of Thanwerdas et al. (2021) and to the final forward simulation of this inversion process with associated optimized fluxes and source signatures. For each test, the model used to simulate Cl concentrations is given. Forward sensitivity tests (FWD-*) have also been run with identical optimized fluxes and source signatures based on the INV-Wang outputs. Note that INV-Wang and FWD-Wang are identical.

Sensitivity Inverse sensitivity test	Forward sensitivity test	Chemistry model	Field name	Modification
SimNoCl-INV-NoCl	FWD-NoCl	None	None	None
INV-NoTropo	FWD-NoTropo	GEOS-Chem v12.09 Wang et al. (2021)	Cl-Wang	No Cl in the troposphere
INV-Wang	FWD-Wang	GEOS-Chem v12.09 Wang et al. (2021)	Cl-Wang	None
SimINCA-INV-INCA	FWD-INCA	LMDz-INCA	Cl-INCA	None
INV-Sherwen	FWD-Sherwen	GEOS-Chem v10 Sherwen et al. (2016b)	Cl-Sherwen	None
INV-Taki	FWD-Taki	CCSR/NIES/FRCGC AGCM v5.7b Takigawa et al. (1999)	Cl-Taki	None

et al., 2021; Karion et al., 2010) and 35 others by the French AirCore programme (Membrive et al., 2017). The balloon-borne AirCore technique (Karion et al., 2010) allows air samples to be taken from the stratosphere (up to approximately 30 km) to the ground, upon a parachute-based descent. Figure S4 and Table S4, in the supplement, provide information about the provider, location and number of profiles collected. Reported uncertainties generally increase with altitude due to end-member mixing within the AirCore samples. They are below 2 ppb in the troposphere and can reach 10 ppb in the lower stratosphere.

We also use air samples from stratospheric balloon flights analyzed in Röckmann et al. (2011) to compare simulated vertical profiles of $\delta^{13}\text{C}(\text{CH}_4)$ to observations. Figure S5 and Table S5, in the supplement, provide information about the time, location and number of profiles collected. The samples were retrieved at four different locations from subtropical to high latitudes, above an altitude of 10 km and up to 35 km. Uncertainties are generally below 0.2 ‰.

2.5 [Estimating global \$\text{CH}_4\$ flux and \$\delta^{13}\text{C}\(\text{CH}_4\)\$ source signature adjustments](#)

Three methods are employed to quantify the influence of the Cl sink on inversions adjusting both CH_4 fluxes and isotopic signatures of sources, here denoted by $\delta^{13}\text{C}(\text{CH}_4)_{\text{source}}$. Simple descriptions of the three methods are provided here whereas comprehensive descriptions are given in the supplement (Text S1, S2 and S3).

The first approach (M1) is based on the INV-* inversions presented in Sect. 2.3 and the 3-D variational inversion system from Thanwerdas et al. (2021). Although this approach is the most robust among the three methods used here, the associated computational burden is also the largest. At present, approximately 4 months are necessary to reach a satisfactory convergence criterion with this system for a 20-year assimilation window, which is highly excessive if one must use this method every

time the influence of two Cl fields are to be compared. Here, we employ this method to show that the two other methods
305 provide global results that are consistent with this robust approach but also to benefit from the high spatial resolution of
the CIF-LMDz-SACS system and therefore perform an analysis at smaller spatial scales. Optimized CH₄ fluxes and source
signatures are directly taken from INV-* results. More information is provided in Text S1.

The second approach (M2) employs a box-model analytical inversion system assimilating both CH₄ and $\delta^{13}\text{C}(\text{CH}_4)$ observations.
This system has been specifically designed for the purpose of this study. The ¹²CH₄ and ¹³CH₄ mole fractions in the troposphere
310 are simulated with this box model, converted to CH₄ mole fractions and $\delta^{13}\text{C}(\text{CH}_4)$ values and compared to globally-averaged
observations provided by the NOAA GML. An analytical non-linear method is then applied to find the optimal solution of the
inversion problem. This method is extremely simple to use and very fast (~ 1 minute) but requires the input parameters of
the box model (global lifetime, KIE and conversion factor between CH₄ mass and mole fractions) to be computed prior to the
inversion. Here, these input parameters are derived from the forward simulations described in Sect. 2.3. More information is
315 provided in Text S2.

The third approach (M3) is not an inversion in its strictest definition. It is only based on an analysis of the time-series of the
bias in CH₄, ¹²CH₄ and ¹³CH₄ total atmospheric masses between two forward simulations (FWD-*) described in Sect. 2.3. This
bias increase over time but stabilize after several decades. We derive a simple theoretical framework to predict the adjustment
value that an inversion system would apply to the prior global CH₄ flux and the globally-averaged $\delta^{13}\text{C}(\text{CH}_4)_{\text{source}}$ in order to
320 offset this bias. More information is provided in Text S3. This method is less robust than the other ones but does not require to
perform an inversion. In Sect. 3.3 and Sect. 3.4, we show that M3 provides results that are very consistent with M1 and M2.

3 Results

3.1 Quantification of the Cl sink

The simulated chemical sink of CH₄ due to Cl oxidation varies depending on the prescribed Cl field. ~~We therefore obtain~~
325 ~~different sink intensities depending on the simulation.~~ Table 4 summarizes the ~~intensities of these sinks~~ multiple estimates
averaged over the ~~simulation 1998-2018~~ period in both the troposphere and stratosphere. Also included in the comparison are
the tropospheric Cl sinks from Hossaini et al. (2016) and Allan et al. (2007), and the stratospheric Cl sink from Patra et al.
(2011). All of them are used in many CH₄ inversions. The Cl sink used in Patra et al. (2011), which is exclusively stratospheric,
is the sum of O(¹D) and Cl sinks. Contributions of O(¹D) and Cl sinks to the stratospheric sink were previously estimated to
330 be 20-40 % and 20-35 %, respectively (McCarthy et al., 2003; Rice et al., 2003). Using these estimates, the Cl sink from Patra
et al. (2011) should contribute between 1.3 % and 2.6 % of the total sink. Using our ~~own~~ estimates of O(¹D) concentrations
obtained with LMDz-INCA (see Sect. 2.1), we obtain a Cl contribution of 2.6 %.

~~From~~ Based on our simulations, contributions from the tropospheric Cl sink with Cl-Wang (0.6 %) and Cl-Sherwen (1.8 %) are slightly lower than those given in the associated papers (i.e., 0.8 % and 2 %, respectively). This discrepancy is likely due
335 to a slight difference in the definition of the tropopause level or/and in the prescribed OH sink that is used to calculate the total
chemical sink.

The tropospheric sink provided by Allan et al. (2007) is well above the other recent values. The tropospheric ~~value from sink estimated by~~ Hossaini et al. (2016), used in recent studies (Saunois et al., 2020; McNorton et al., 2018), is also slightly above that ~~of inferred with~~ CI-Sherwen (Table 4: 1.4 times higher) but well above ~~that of those inferred with~~ CI-Wang and CI-INCA (4 and 8.5 times higher). In the troposphere, the sink ~~induced by~~ ~~inferred with~~ CI-Taki is much larger than the other sinks (up to 28 times larger) and therefore even larger than the value suggested by Allan et al. (2007) which is ~~already~~ very likely to be overestimated (Gromov et al., 2018). In the stratosphere, ~~the this~~ CI-Taki sink is also slightly larger ~~than the others~~ (1.3 times that of CI-Sherwen).

Apart from the CI-Taki field, ~~we selected here only the fields that provided a realistic range of concentrations when applying all the fields provide a range of tropospheric concentrations that are roughly in line with~~ the conclusions of Gromov et al. (2018). ~~We therefore consider only the CI fields that give a tropospheric oxidation below 2% as realistic. These fields happen to be the most recent and up-to-date estimations.~~ In the stratosphere, all tested fields ~~are considered realistic because they~~ provide an oxidation between 1.1 and 1.6 %, ~~therefore~~ in agreement with Saunois et al. (2020) and McCarthy et al. (2003) (0.4-2.4 %). ~~In the following analysis, results from SimTaki are presented only to illustrate why a CI field should be rigorously analyzed (concentration, oxidation) before prescribing it in a forward or inverse simulation.~~

Table 4. Percentage of contribution from CI oxidation to total chemical oxidation (CI, O(¹D) and OH) ~~and~~, sink ~~intensity~~ ~~intensities and mean CI concentration (conc.)~~. Values are given for the tropospheric, stratospheric and total (tropospheric + stratospheric) CI sinks for several fields, either used in the simulations or in other studies. * Values taken from literature. H16 : Hossaini et al. (2016) ; A07 : Allan et al. (2007) ; P11 : Patra et al. (2011)

Field	Troposphere			Stratosphere			Total	
	Oxidation (%)	Sink (TgCH ₄ .yr ⁻¹)	Conc. (molec.cm ⁻³)	Oxidation (%)	Sink (TgCH ₄ .yr ⁻¹)	Conc. (molec.cm ⁻³)	Oxidation (%)	Sink (TgCH ₄ .yr ⁻¹)
SimNoCH INV-NoCl	0	0	0	0	0	0	0	0
SimNoTropo INV-NoTropo	0	0	0	1.1	6.1 <u>5.8</u>	1.5 × 10 ⁵	1.1	6.1 <u>5.8</u>
SimINCA INV-INCA	0.3	1.5 <u>1.4</u>	3.3 × 10 ²	1.0	5.2 <u>5.0</u>	1.4 × 10 ⁵	1.2 <u>1.3</u>	6.7 <u>6.4</u>
SimREF INV-Wang	0.6	3.2 <u>3.0</u>	6.1 × 10 ²	1.1	6.1 <u>5.8</u>	1.5 × 10 ⁵	1.7	9.3 <u>8.8</u>
SimSherwen INV-Sherwen	1.8	9.9 <u>9.3</u>	1.1 × 10 ³	1.2	6.4 <u>6.0</u>	1.6 × 10 ⁵	3.0	16.3 <u>15.3</u>
H16*	2.6	12-13	1.3 × 10 ³	N/A	N/A	N/A	N/A	N/A
A07*	5	25	N/A	N/A	N/A	N/A	N/A	N/A
SimTaki INV-Taki	8.5	47.0 <u>46.8</u>	4.7 × 10 ³	1.6	9.0 <u>8.9</u>	2.1 × 10 ⁵	10.1	56.0 <u>55.7</u>
P11*	N/A	N/A	N/A	1.3-2.6	6.8-13.7	N/A	N/A	N/A

3.2 ~~CH₄ surface concentrations~~ Spatial distributions of biases

~~The impact of the CI sink on Figure 2 shows the CH₄ mole fractions is analyzed by comparing the simulations against SimREF at MBL station locations providing and δ¹³C(CH₄) data. Since the CI fields vary mainly as a function of latitude, surface absolute biases between the simulations and the FWD-Wang averaged over the period 2010-2018. For CH₄, globally-averaged~~

355 biases range from -18 ppb to 123 ppb because prescribed Cl sinks are distinct. However, the spatial variations of biases around their mean value are similar for FWD-Taki, FWD-INCA and FWD-Sherwen since all the fields exhibit similar spatial patterns. For all biases, the minimum-maximum relative difference is below 5 %. Some biases are low enough for us to see the influence of surface fluxes (local CH_4 enhancements) on biases in Fig. 2 (blue tropical regions in FWD-INCA and FWD-NoTropo panels). This is not visible in the bias corresponding to FWD-Sherwen and FWD-Taki as the comparisons are made by averaging values over bands of latitude. Here, the bias b is defined as :

$$b_{X,i,l} = \overline{X_{i,s}} - X_{\text{SimREF},s}^l$$

365 minimum-maximum difference is larger. Tropospheric Cl concentrations are generally larger in the tropics and therefore the bias between FWD-NoTropo and FWD-Wang is also larger in this latitudinal band. However, further removing the stratospheric Cl (FWD-NoCl) invert the spatial distribution of the bias, hence leading to higher values in the polar regions. Following the Brewer-Dobson circulation, stratospheric air descends into the troposphere mainly in polar regions (Butchart, 2014). The influence of stratospheric Cl on tropospheric CH_4 mole fractions is therefore enhanced in these regions. To summarize, although spatial variations exist and can be slightly different from one field to another, they generally remain below 1 ppb and can be neglected.

370 where $b_{X,i,l}$ is the bias for a specific quantity X (i. e., or Δs for $\delta^{13}\text{C}(\text{CH}_4)$), a specific simulation i , and a specific band of latitude l . $\overline{X_{i,s}}$ denotes the or, globally-averaged biases are larger than the recent global decline in $\delta^{13}\text{C}(\text{CH}_4)$ values simulated by a simulation i and at a station s . The $\overline{(\cdot)}^l$ symbol indicates the mean over all the stations whose location is inside the band of latitude l .

375 In a box model, the temporal evolution of the observed since 2007 (Nisbet et al., 2019). Although mean values highly differ from one simulation to another, spatial variations are very similar and we find the lowest values where the sources with the most depleted isotopic source signatures are located, e.g., in boreal regions (wetlands) and in Asia (agriculture and waste). These spatial discrepancies are mainly caused by the non-linear effects associated with isotopes. In a very simple framework, we can demonstrate that the steady-state bias $\Delta\delta_0$ between two simulations prescribing the same CH_4 budget for a simulation i is described by the equation below : source and the same source signature δ_s is given by the formula :

$$\frac{dB_i}{dt} = S\Delta\delta_0 \approx -\frac{B_i}{\tau_i} \Delta\epsilon \cdot (1 + \delta_s) \quad (2)$$

380 where B_i is the mass of in the atmosphere in, S is the source in and τ_i is the chemical lifetime of in the atmosphere in. Note that the same sources are prescribed for all simulations. The temporal evolution of the budget is not linear, because the sink is proportional to mole fractions. decrease/increase induces a negative feedback on the magnitude of the sink, leading to a stabilization of $\Delta\epsilon$ denotes the difference of prescribed fractionation between the two simulations due to differences in Cl concentrations. More information and a comprehensive demonstration are provided in Text S4. Consequently, the bias will be lower if the source is more depleted in ^{13}C . Figure 2 confirms that these non-linear effects have a larger influence on the spatial patterns of the bias than stratospheric air intrusions, spatial differences between Cl concentrations or even horizontal transport. In addition, the mass of after several decades if S bias between FWD-NoTropo and τ_i are constant over time. Here, the bias

between two simulations is caused by a change in τ because we modify the Cl field. The evolution of the bias b can therefore be described by the equation \div :

$$390 \quad \frac{db}{dt} = \frac{d(B_2 - B_1)}{dt} = -\frac{B_1}{\tau_1} + \frac{B_2}{\tau_2}$$

However, in FWD-NoCl is a surface-based inversion (i.e., an inversion assimilating observations from surface stations) without sink optimization, the bias is compensated by a correction of the global surface flux $S + \Delta S$. The inversion system therefore answers the question: "What is the good proxy for quantifying the influence of stratospheric Cl on $\delta^{13}\text{C}(\text{CH}_4)$ at the surface. At the end of the period, STE cause a globally-averaged increase of $\delta^{13}\text{C}(\text{CH}_4)$ at the surface of $0.30 \pm 0.01 \text{‰}$ (depending on the region) when the stratospheric Cl concentrations from Wang et al. (2021) are adopted. Although this value could change with another field, our range of stratospheric Cl concentrations is small and the Cl-Wang field is taken from the most comprehensive and recent study to date. Therefore, we think that this value is a good estimate of the contemporary influence of stratospheric Cl on $\delta^{13}\text{C}(\text{CH}_4)$ at the surface. It is larger than the estimate of Wang et al. (2002) inferred between 1970 and 1992 (0.23‰). Both our estimates were obtained after running a model for about the same amount of years, therefore these values are comparable. In addition, Wang et al. (2002) experimented with multiple configurations. In particular, one of the runs tested an enhanced STE, resulting in a value of ΔS that will offset the bias caused by 0.38‰ . Another test, with stratospheric Cl concentrations increased by a factor 2, provided a value of 0.32‰ . However, the latter study does not provide an estimate of the mean stratospheric Cl concentration. It is therefore difficult to know whether the discrepancy between both estimates are due to Cl stratospheric concentrations, the rate of STE or something else. Our value however lies within the full range obtained by Wang et al. (2002)

405

3.3 Global CH₄ flux adjustment

The global CH₄ flux adjustments resulting from a change in the prescribed sink? ". The temporal evolution of the bias between a simulation-Cl sink have been derived using the three methods introduced in Sect. 2.5 (Fig. 3). The INV-Wang simulation has been chosen as a reference. Global CH₄ flux adjustments range from $-7.0 \text{ TgCH}_4 \cdot \text{yr}^{-1}$ (no Cl sink) to $+46.8 \text{ TgCH}_4 \cdot \text{yr}^{-1}$ (Cl-Taki) with M1. Small differences between M1 and the other methods exist (up to 10%). However, the strong similarity between these results confirms that M2 and M3 can be employed to investigate the influence of the Cl sink on inversion-based adjustments for the global scale without significantly impacting the magnitude or sign of the results. This result corresponding to Cl influence may not be valid for larger changes such as those resulting from an OH sink modification. With the M1 method, more information about the spatial characteristics of the flux adjustment can be provided. About 70 % of the adjustment is made in the reference simulation can therefore be described by the equation \div :

415

$$\frac{db}{dt} = \Delta S - \frac{b}{\tau_{ref}}$$

τ_{ref} denotes the chemical lifetime in the reference simulation. We consider that ΔS is constant over time as the inter-annual variability of the Cl sink is below 0.4. In that case, tropics (30°S - 30°N) and the rest in the northern mid-latitudes (30°N - 60°N).

The other regions of the solution of this equation is :-

$$420 \quad b(t) = \Delta S \times \tau_{ref} \times \left(1 - e^{-\frac{t}{\tau_{ref}}}\right)$$

The value of ΔS can be obtained by analyzing the temporal evolution of the bias and, in particular, by looking at the value of the bias when it is stabilized (steady state). Here, after 21 years of simulation, the stabilization is not reached yet (see Fig. ??, top row). Therefore, we choose to extend our results by applying a curve fitting function to our simulated values :-

$$b_{X,i,l}(t) = A_{X,i,l} \times B_{X,i,l} \times \left(1 - e^{-\frac{t}{B_{X,i,l}}}\right)$$

425 $A_{X,i,l}$ and $B_{X,i,l}$ are two constants that the curve fitting algorithm returns world contribute only to a few percents of the global adjustment. This is consistent with the spatial distribution of the biases presented in Sect. 3.2. Also, changing the reference scenario does not modify this distribution.

Using this sample of results, we have also build a linear regression model in order to maximize the agreement between the simulated values and the curve fitting function. Using this function, the results are extended until 2070 to reach a clear 430 stabilization of simulated biases (see Fig. ??, top row).

At steady state, the bias of easily predict the influence of changing the CI field on the global CH_4 at the surface varies between -20.0 flux adjustment. By performing a linear regression between the adjustment values inferred with M1 and the mean tropospheric CI concentrations, we obtain a coefficient of determination R^2 very close to 1. It indicates that a linear relationship is a very good approximation of the relationship between the two variables. Consequently, one can affirm that 435 each increase by 1000 for SimSherwen and 24.5 for SimNoCI (Table ??, second column). An estimation of ΔS is given by the coefficient $A_{X,i,l}$. It provides a result in . To convert this value in , we use a conversion factor of 2.767 (Lassey et al., 2000) and show the final estimates in Table ??, fourth column. For SimNoCI and SimSherwen, these estimations are molec.cm⁻³ in the mean tropospheric CI concentration would require an adjustment of +11.7 TgCH₄.yr⁻¹. It represents a change in about 2 % of total CH₄ atmospheric oxidation, which is very small compared to the current uncertainties in OH sink intensity and their 440 influences on top-down estimates (Zhao et al., 2020, 2019). Furthermore, the discrepancies between the mean tropospheric CI concentrations estimated by recent studies are generally smaller than 1000 molec.cm⁻³. Therefore, the uncertainty on CH₄ emission estimates arising from the choice of CI sink should not be larger than 11.7 TgCH₄.yr⁻¹. However, inverse modellers should be extremely cautious before using CI fields that exhibit much larger CI concentrations than recent estimates. As shown here, it can cause the flux adjustment to reach 50 TgCH₄.yr⁻¹.

445 As the inversion compensates for the sink difference induced by a change from one field (CI-1) to another (CI-2), the numerical value of the global flux adjustment is very close (difference of less than 0.2 less than a 10 % difference) to the tropospheric CI sink discrepancies from Table 4. Indeed, as the stratospheric CI sinks in SimREF, SimINCA, SimNoTropo and SimSherwen are almost identical, the biases induced by tropospheric CI sink discrepancies will be logically compensated by a source adjustment of the same intensity as the sink discrepancy. For SimNoCI, the biases at the surface are also influenced 450 by large stratospheric sink discrepancies. Therefore, the inferred adjustment values cannot be so simply related to the sink discrepancies. Also, latitude has a very low influence on biases and adjustment values, causing a variation of less than 5 % around the mean value (see Fig. ??).

We conclude that a source adjustment of 12.3 difference between estimated tropospheric sink intensities for CI-1 and CI-2 (see Table 4). The stratospheric sink appears to have also a small influence on the results. For instance, between INV-NoCl and INV-NoTropo, there is a global flux adjustment of $3.8 \text{ TgCH}_4.\text{yr}^{-1}$ would be necessary between a surface-based inversion without CI sink, such as the inversions carried out with LMDz-SACS up to now, and a surface-based inversion adopting the CI-Sherwen field. Saunois et al. (2020) obtained an uncertainty on the total, resulting only from the difference in stratospheric CI sink. It is significantly smaller than the stratospheric sink itself because a fraction of CH_4 fluxes of about 40 does not return to the troposphere from the stratosphere. In addition, stratospheric influence is not always the only cause of discrepancies. For instance, the global flux adjustment obtained with INV-Taki is $48.8 \pm 5.8 \text{ TgCH}_4.\text{yr}^{-1}$ (maximum – minimum difference) across the different top-down inversions reported. The difference in the CI configuration between the multiple inversions of Saunois et al. (2020) may have contributed to the uncertainty they estimated. Although the adjustment value we obtain here thus remains lower than the uncertainty generated by the different configurations used in Saunois et al. (2020), it is not negligible as we make the point that this source adjustment could be much larger if an unrealistic CI field was used. For example, prescribing the and the difference between the estimated total (tropospheric and stratospheric) sinks is $47.0 \pm 0.8 \text{ TgCH}_4.\text{yr}^{-1}$. Therefore, differences between the estimated sinks cannot explain alone the global flux adjustment. It is very likely that if the spatial distributions of two tropospheric CI sinks are different, it can cause such discrepancies. CI-Taki field instead of the CI-Wang field would result in an adjustment value of 48.1. If a single CI configuration for all inversions could be agreed upon, this would likely lead to a reduction of the uncertainty on emission fluxes infers a larger proportion of its total sink in the tropics compared to CI-Wang. However, the total chemical lifetime of CH_4 is smaller in the tropics than in the high-latitudes. Therefore, the inversion system must increase even more the CH_4 flux in this region to compensate for these spatial distribution discrepancies. This effect remains nevertheless extremely small. For the other simulations, it is very difficult to separate the influence of the stratospheric sink from the influence of discrepancies arising from spatial distribution.

As the stratospheric CI concentrations estimated by the models presented here suffer much less uncertainties than the tropospheric CI concentrations, we did not investigate the influence of the variations in stratospheric CI. However, note that M2 and M3 have difficulties reproducing the M1 value when we remove entirely the CI sink (NoCl bars in Fig. 3). It confirms that the stratospheric influence of CI cannot be well captured by a box model framework.

Global adjustment values of source and isotopic signatures inferred from and biases at the surface. Second column is the global bias at the surface and at steady state. Third column is the global bias at the surface and at steady state. Fourth column is the global source adjustment value estimated using the methods described in Sect. ???. Fifth column is the source adjustment value estimated using the methods described in Sect. ???. Latitudinal dependency is reported as a minimum–maximum range min/max for all values. Flux Signature () () () SimNoCl 24.5 24.4 / 24.8 –0.66 –0.70 / –0.63 –5.7 –5.7 / –5.70.66 0.63 / 0.70 SimNoTropo 10.0 10.0 / 10.0 –0.30 –0.31 / –0.28 –3.2 –3.2 / –3.20.30 0.28 / 0.31 SimINCA 8.6 8.6 / 8.8 –0.25 –0.26 / –0.24 –1.9 –2.0 / –1.90.25 0.24 / 0.26 SimSherwen –20.0 –21.2 / –20.50.60 0.59 / 0.626.6 6.5 / 6.8 –0.60 –0.62 / –0.59 SimTaki –140.1 –142.2 / –138.24.13 4.01 / 4.2448.1 46.9 / 49.2 –4.13 –4.24 / –4.01

3.4 Global $\delta^{13}\text{C}(\text{CH}_4)$ signal at the surface_{source} source signature adjustment

In contrast with the biases, the biases between the simulations are much larger than recent observed downward shifts (~ 0.3). Our methods are also designed to derive the global $\delta^{13}\text{C}(\text{CH}_4)_{\text{source}}$ source signature adjustment resulting from a change in prescribed Cl field. Figure 3 provides a comparison of the results with the three different methods. Global $\delta^{13}\text{C}(\text{CH}_4)_{\text{source}}$ adjustments range from -4.1 ‰ since 2007). We use the same curve fitting method as before to propagate the time-series until 2070 in order to reach a steady state (see Fig. ??, bottom row).

SimNoTropo, SimINCA, SimREF and SimSherwen have very similar stratospheric Cl sinks (Table 4). Therefore, biases for SimNoCl, SimNoTropo, and SimSherwen are mostly generated by discrepancies in tropospheric Cl sink intensity. We can estimate that each percent increase in how much is oxidized by Cl leads to an additional 0.53 (Cl-Taki) to $+0.6$ ‰ increase in, therefore larger than the global downward shift observed since 2007. After 14 years of simulation, we obtain a value of 0.46 , (no Cl sink) with M1. M2 and M3 results are highly consistent with M1 results, showing that simpler methods can also capture the $\delta^{13}\text{C}(\text{CH}_4)_{\text{source}}$ adjustment. A linear regression model has also been built to quantify the relationship between the $\delta^{13}\text{C}(\text{CH}_4)_{\text{source}}$ adjustment and the mean tropospheric Cl concentration. We obtain a coefficient of determination R^2 very close to the value of 0.51 and estimate that a $\delta^{13}\text{C}(\text{CH}_4)_{\text{source}}$ adjustment of -1.0 ‰ inferred by Strode et al. (2020) after the same number of years.

Stratospheric Cl also influences at the surface through STE. We estimate this influence using the bias between SimNoCl and SimNoTropo. Intrusions of stratospheric air are therefore responsible of an enrichment at the surface stations of 0.30 ± 0.04 ‰ would result from each increase by 1000 (depending on the latitude) after 21 years of simulation, larger than the value of Wang et al. (2002) inferred between 1970 and 1992 ($0.23 \text{ molec. cm}^{-3}$ in the mean tropospheric Cl concentration to compensate for the enhanced atmospheric isotopic fractionation. Based on the Cl fields analyzed here, the globally-averaged $\delta^{13}\text{C}(\text{CH}_4)_{\text{source}}$ should very likely lie in the range of $[-56.7, -51.9]$ ‰).

To reduce these biases to zero, an inversion system would adjust the globally-averaged isotopic signature of the sources, denoted by source . This adjustment factor would be roughly equal to the opposite of the bias at steady state (see demonstration in the supplementary Text S2). It would therefore oscillate between . If one excludes outliers such as Cl-Taki or no Cl at all, we deduce a likely range of $[-0.6053.1, -52.2]$ ‰ (SimSherwen) and $+0.66$ for the period 1998-2018. This range does not account for other uncertainties, e.g., uncertainties in the numerical value of the KIE associated with the OH sink.

We find a difference of 0.30 ‰ (SimNoCl) around the mean isotopic signature of the between global $\delta^{13}\text{C}(\text{CH}_4)_{\text{source}}$ inferred with INV-NoCl and INV-NoTropo, confirming the influence of stratospheric Cl on $\delta^{13}\text{C}(\text{CH}_4)$ at the surface first estimated in Sect. 3.2. This effect must be rigorously accounted for when using one-box modelling to estimate global CH_4 source prescribed in SimREF. We would therefore obtain, after the inversion process, a mean global signature between -53.20 (SimSherwen) and -51.94 (SimNoCl).

The system would modify emissions and dealing with isotopic constraints because it is comparable to the recent global decline in $\delta^{13}\text{C}(\text{CH}_4)$ observed since 2007 (Nisbet et al., 2019). These results highlight that preferring a Cl field over another can highly influence the posterior globally-averaged $\delta^{13}\text{C}(\text{CH}_4)_{\text{source}}$ by changing of an inversion performed with isotopic constraints. As the globally-averaged $\delta^{13}\text{C}(\text{CH}_4)_{\text{source}}$ mainly depends on the source mixture and/or the isotopic signatures of the multiple emission categories, with a weight depending on uncertainties associated to both. For instance, an adjustment

of -0.60 could be made by increasing the wetlands share from 32% , contributions from emission categories to 43% or by shifting the mean isotopic signature of wetlands from -56.6 to -58.5 , more in agreement with recent estimates (Ganesan et al., 2018; Sherwood et al., 2017) than our inverted value (see Table ??). However, the system would likely change not only wetlands but all emission categories, possibly limiting an unlikely large change in wetlands emissions only. Nevertheless, the configuration used to represent the Cl sink could largely influence the result of an inversion assimilating both and total emissions can be highly affected by a modification of the prescribed Cl field. In our inversions, WET, BB, FFG and AGW emissions contribute between $[32.5, 33.3]\%$, $[4.9, 5.2]\%$, $[21.0, 21.5]\%$ and $[37.3, 37.6]\%$, respectively. For wetlands, such a variation roughly corresponds to a $15 \text{ TgCH}_4 \cdot \text{yr}^{-1}$ change, resulting only from uncertainties in Cl concentrations. Furthermore, our inversions optimize the source signatures prescribed for each category and account for a relatively large uncertainty in prior estimates. Consequently, it releases part of the constraint that could be applied on the source mixture in an inversion not optimizing source signatures. Our results are therefore a lower-bound estimate of the influence of the Cl sink on top-down estimates with isotopic constraints. It emphasizes how careful one must be when selecting a prescribed Cl field for running such inversions.

Seasonal cycles of and biases between the surface values simulated by the various simulations (see Sect. ??) and those simulated by SimREF. The biases are averaged over four bands of latitude.

3.5 CH_4 and $\delta^{13}\text{C}(\text{CH}_4)_{\text{4}}$ seasonal cycles

To investigate the seasonal cycle, the simulations are compared against SimREF by averaging values over latitudinal bands. The peak-to-peak amplitude of the CH_4 seasonal cycle simulated by FWD-Wang at the surface typically ranges between 5 and 120 ppb, depending on the region (see Fig. ??) as in Sect. ?? and ??.

With the realistic Cl fields tested here, the influence on the seasonal cycle is negligible regardless of the latitudinal band analyzed. The variation in the seasonal cycle amplitude due to Cl is about 0.4 ppb whereas the seasonal cycle amplitude is about 20 in the Southern Hemisphere and 30 S6, in the supplement). It is larger where wetlands and biomass burning emissions are located because both sources exhibit a very strong seasonal dependence. Apart from using the Cl-Taki, changing the prescribed Cl field does not modify the amplitude and the spatial variability of the CH_4 seasonal cycle. Compared to FWD-Wang, the variation is below 3% in both hemispheres for FWD-Sherwen, FWD-INCA, FWD-NoTropo and FWD-NoCl. However, it can reach 10% in the Northern Hemisphere. The variation therefore accounts for $1-2\%$ of when applying Cl-Taki instead of Cl-Wang.

As for $\delta^{13}\text{C}(\text{CH}_4)_{\text{4}}$, the seasonal cycle amplitude is simulated by FWD-Wang typically ranges between 0.05 and 0.65% . Again, changing the prescribed Cl field has more influence on $\delta^{13}\text{C}(\text{CH}_4)_{\text{4}}$ seasonal cycle and is dependent on latitude. In than on CH_4 . For instance, in the Southern Hemisphere, the variation in amplitude between SimREF and SimSherwen when switching from Cl-Wang to Cl-Sherwen is about 0.02% , which represents 20% of the total seasonal cycle amplitude. In the Northern Hemisphere, the variation can exceed 0.03% , which represents but it represents only 10% of the seasonal cycle amplitude.

555 ~~SimTaki (not shown on Fig. ?? for clarity reason) causes a much larger variation in seasonal cycle for both and . For ,~~
~~variations reach 5~~ Adopting the CI-Taki field drastically increases this variation in the amplitude of the seasonal cycle: variations
can go up to 99 % in the Southern Hemisphere and 1058 % in the Northern Hemisphere. ~~As , with large spatial disparities.~~
Also, differences of amplitudes for $\delta^{13}\text{C}(\text{CH}_4)$; ~~variations go up to 99~~ between INV-NoTropo and INV-NoCl reach 10 % in the
~~Southern Hemisphere and 58 % in the Northern Hemisphere~~ tropics and are negligible in other regions. It indicates that STE
560 ~~tends to slightly increase the seasonal cycle around the equator when stratospheric Cl is included.~~

The influence of Cl on ~~the simulated~~ $\delta^{13}\text{C}(\text{CH}_4)$ seasonal cycle must be considered as it ~~will impact~~ ~~impacts~~ the results of
an inversion with ~~data assimilation~~ isotopic constraints. A misrepresentation of the seasonal cycle forces the system to adjust
the intensity of sources that ~~actively participate in~~ ~~exert a large influence on~~ the seasonal cycle, such as wetlands or biomass
burning ~~emissions. This influence is negligible for and noticeable for when keeping realistic Cl concentrations but becomes~~
565 ~~very large when using other Cl fields, such as the CI-Taki field. Using the MI method presented above, one can analyze the~~
~~influence of prescribed Cl sink on optimized emissions for all categories. Apart from INV-Taki, the variation of peak-to-peak~~
~~amplitude of the seasonal cycle for global emissions and for each category is small between INV-Wang and all the other inverse~~
~~configurations. It is below 5 % for WET, AGW, NAT and FFG but can reach 10 % for BB. On the contrary, INV-Taki infers~~
~~much larger amplitude changes. BB, WET, AGW, NAT and FFG seasonal cycle amplitudes are increased by 3.1, 2.0, 0.1, 0.1~~
570 ~~and 0.2 TgCH₄.yr⁻¹ (134, 14, 9, 1 and 21 %), respectively.~~

3.6 CH₄ vertical profiles

~~Vertical~~ At present, vertical profile measurements of CH₄ are too scarce to be considered as a stand-alone constraint in inversion
systems, and so are rather used as evaluation data. Nevertheless, as their accuracy, spatial coverage and number increase,
their assimilation will become increasingly relevant. It is, however, necessary to increase the model-observation agreement,
575 especially in the stratosphere, before considering their assimilation. We analyze here the influence of the Cl ~~configuration~~
~~on these~~ ~~distribution on the simulated~~ profiles. We also compare the simulated vertical profiles to observations to investigate
whether modifying the Cl ~~configuration~~ ~~distribution~~ can help to reduce the model-observation discrepancies.

Simulated vertical profiles are sampled at the same locations and ~~time as the observations available . The bias~~ ~~b_{X,y,p,d_1,d_2}~~
~~between two vertical profiles d_1 and d_2 (simulated or observed) times as the available observations. Simulations with optimized~~
580 ~~fluxes (INV-*) are used to reduce the influence of a potential tropospheric bias resulting from a poor estimation of the CH₄~~
~~fluxes and to analyze to what extent a station-based inversion can help to reduce both the tropospheric and stratospheric biases.~~

~~The bias b_p between observed (obs) and simulated (sim) values for a specific profile p , a specific quantity X (i.e., and for~~
 ~~$X = \text{CH}_4$) and is given by:~~

$$585 \quad b_p = X_{p,sim} - X_{p,obs} \quad (3)$$

We define the mean bias $\overline{b_{r,p}^y}$ for a specific layer y (troposphere, stratosphere or total) is given by:

$$b_{X,y,p,d_1,d_2} = \overline{X_{d_1,p} - X_{d_2,p}}^y$$

The $\overline{(\cdot)}^y$ symbol indicates the mean column) and a specific region of interest r as the root-mean square difference (RMSD) over all the vertical levels in the layer y . We also define the mean bias as the bias averaged over all available vertical profiles:

590 $\overline{b_{X,y,d_1,d_2}} = \overline{b_{X,y,p,d_1,d_2}}^p$

values of the bias in this layer and in this region.

Table 5. Mean bias relative to SimREF for RMSD between simulated and observed CH₄ vertical profiles in the troposphere and stratosphere as well as in for different regions of the Northern and Southern Hemisphere world.

Simulation	Troposphere				Stratosphere			
	Northern high-latitudes	Mid-latitudes USA	Mid-latitudes Europe	Southern Hemisphere	Northern high-latitudes	Mid-latitudes USA	Mid-latitudes Europe	Southern Hemisphere
	ppb							
SimNoCl-INV-Wang	3.0	15.6	21.9	16.7	106.8	81.4	93.0	67.4
INV-Taki	2.3	16.0	19.3	19.1-15.1	50.8-111.7	38.9-75.4	86.2	71.6
SimNoTropo-INV-Sherwen	10.9-2.9	10.8-14.6	15.2-22.4	12.9-15.4	109.8	81.6	93.2	69.0
SimINCA-INV-INCA	6.8-3.3	6.7-16.2	11.8-21.7	9.2-17.6	108.6	86.2	98.2	66.9
SimSherwen-INV-NoTropo	-18.7-3.5	-18.2-16.3	-18.1-21.7	-17.9-17.4	106.6	81.1	92.5	67.2
SimTaki-INV-NoCl	-129.7-4.4	-125.0-17.0	-118.5-21.8	-121.4-18.4	115.5	103.6	118.6	67.5

The mean bias relative to SimREF is given for all simulations and observations in Table???. A change in the Cl field (and keeping it realistic) induces a maximum mean bias of 51 in the stratosphere (SimNoCl). For all simulations besides SimNoCl, the bias is roughly constant over the entire column (see Fig. ???), because the Cl concentrations in the stratosphere are very similar. Also, a change in the tropospheric Cl sink influences tropospheric and stratospheric values to the same magnitude. For SimNoCl, the bias is constant in the troposphere but starts increasing above 15 km at 7.5 in the Northern Hemisphere and 7 in the Southern Hemisphere. At 25 km, the bias therefore reaches 130 ppb in the Northern Hemisphere for this simulation

Table 5 shows the mean bias for four regions of the world where vertical profiles have been observed : northern high-latitudes in Europe, mid-latitudes in Europe, mid-latitudes in the USA and Southern Hemisphere (Oceania). After inversion adjustments, tropospheric CH₄ is well captured by the model. Biases are particularly low in the northern high-latitudes, albeit the number of profiles (4) is much lower in this region and additional data should be used to confirm this result. In the other regions, values are larger mainly because models have difficulties reproducing observed values very close to the surface. It is likely due to a problem of representation of transport in the boundary layer in LMDz-SACS and/or a problem of spatial representativity of sources that can be resolved only by increasing spatial resolution. Simulated profiles are generally slightly overestimated in Europe and underestimated in the USA in the troposphere, albeit by less than 10 ppb. Overall, the prescribed Cl field has very

little impact on the tropospheric mean biases. Discrepancies between Cl fields for a given region are too small to validate one Cl field over another.

610 Model-observation discrepancies reaches 250 (around 20 and 25 km) in both Hemispheres. Root Mean Square Error (RMSE) Mean biases are much larger in the stratosphere is 102 ± 21 in the Northern Hemisphere and 84 ± 15 in the Southern Hemisphere for SimREF. For all simulations, inflections of mole fractions observed at 15 and 20 km, ranging from about 67 ppb in the southern high-latitudes to 115 ppb in the northern high-latitudes. Outside the northern high-latitudes, simulated values are generally larger than observed values for all simulations and all regions, showing that the model tends to overestimate CH₄ mole fractions, even with optimized fluxes. Influences of the Cl sink are larger in the stratosphere for the four regions. INV-NoCl has more difficulties reproducing the simulated mole fractions above the tropopause, mainly in the Northern Hemisphere are simulated 5 km higher (~ 20 and 25 km) than observed. These misrepresentations lead to simulated vertical gradients between 15 and 25 km much stronger than observed (900 against 650 in the Northern Hemisphere). Unfortunately, with a mean bias 1.0 to 1.4 times larger than the other simulations. INV-Taki shows the lowest biases in the mid-latitudes, indicating that the stratospheric Cl concentrations could be underestimated in most of the tested fields in this region. However, this overestimation of CH₄ mole fractions in the stratosphere could be also caused by an underestimation of the stratospheric OH or O(¹D) concentrations or a weak transport between troposphere and stratosphere, preventing the tropospheric CH₄ to reach higher altitudes. Such a misrepresentation can also result in an overestimation of the column-weighted average mixing ratio (XCH₄) simulated by LMDz-SACS (Ostler et al., 2016). An analysis of XCH₄ is however beyond the scope of this study. Overall, modifying the prescribed Cl field does not correct these errors. Cl field has a very limited impact on simulated CH₄ vertical profiles as long as its stratospheric concentrations remains in the range analyzed here.

625 3.7 $\delta^{13}\text{C}(\text{CH}_4)$ vertical profiles

Although modifying the prescribed Cl field can induce local differences in stratospheric mole fractions of the same order of magnitude as the model errors, none of Figure 5 displays the comparison between observed vertical profiles of $\delta^{13}\text{C}(\text{CH}_4)$ from Röckmann et al. (2011) and those simulated by the INV-* runs. As most of the tested Cl sink really improves our model-observation agreement observed profiles were retrieved before the beginning of our simulations, we selected the year 2005 for the comparison. Although our inversions did optimize initial conditions, constraints from surface stations do not carry enough information to efficiently optimize stratospheric $\delta^{13}\text{C}(\text{CH}_4)$. Therefore, a stabilization period in response to the prescribed Cl sink is necessary. However, in the stratosphere as the inflections of mole fractions are not properly represented. Patra et al. (2011) already mentioned that strong vertical gradients of around the tropopause may be caused by a too slow Brewer-Dobson circulation so these discrepancies are possibly due to transport errors rather than errors in removal rates. Further investigating the discrepancy in the stratosphere is however beyond the scope of this study, this stabilization is somehow very fast (about 2-3 years) and the year selected for comparison has a negligible influence on the analysis. Selecting 1998 or 1999 slightly influences the comparison but does not affect the conclusions.

Ostler et al. (2016) showed that model errors in simulating stratospheric CH₄ contribute to model biases when compared to observed column-averaged CH₄ dry-air mole fractions (XCH₄) from the Total Carbon Column Observing Network (TCCON).

640 ~~XCH₄ obtained by remote sensing techniques are now massively assimilated in inversions because satellite observations offer a much larger spatial coverage than in situ measurements. Rigorously estimating the influence of Cl concentrations on a satellite-based inversion would require more than an one-box model approximation. We therefore include only a simple analysis using data from the GOSAT satellite in the supplementary Text S3~~ Apart from INV-NoCl, our simulations capture well the observed profiles. Vertical profiles of $\delta^{13}\text{C}(\text{CH}_4)$ that are simulated without any Cl sink are the most inconsistent with available
645 observations. RMSDs of INV-NoCl over KIR, ASA, and GAP are respectively 1.5, 2.2, and 2.5 times higher than the mean RMSD over the other simulations and over the same locations. Furthermore, the differences between Cl-INCA, Cl-Sherwen, Cl-Wang have little influence on the vertical profiles of $\delta^{13}\text{C}(\text{CH}_4)$ due to the fact that the stratospheric Cl concentrations are relatively close ($1.4\text{--}1.6 \times 10^5 \text{ molec.cm}^{-3}$). Vertical profiles are well captured up to 30-35 km for ASA, HYD, and GAP, confirming that the prescribed Cl concentrations in the lower stratosphere are realistic (average RMSDs of 1.0, 0.5, and 1.5 ‰).
650 Cl-Taki stratospheric concentrations are slightly larger than the others and, therefore, simulated $\delta^{13}\text{C}(\text{CH}_4)$ is higher above 30-35 km for all regions.

Above KIR, in the polar regions, the simulated values are less consistent with observations (mean RMSD of 4.2 ‰). Several explanations can be given. First, Cl concentrations may be underestimated in the lower stratosphere and in the polar regions. Secondly, the transport between the lower and upper stratosphere may not be correctly represented in the LMDz model, leading
655 to a poor mixing between layers above the tropopause with ¹³C-enriched CH₄ and more depleted layers below the tropopause. However, there is a high variability in the 7 profiles analyzed above KIR (light gray band), and the simulated values are within the uncertainty of these observations. Overall, available observations are limited to approximately 30 km and the influence of the prescribed Cl sink on the simulations is much clearer above this altitude. It is therefore difficult to prefer one Cl field over another without observing at higher altitudes.

660 4 Conclusions

In this study, we tested ~~multiple Cl fields suggested by recent studies~~ a large range Cl concentration fields in order to investigate the influence of the Cl ~~configuration distribution~~ on CH₄ and $\delta^{13}\text{C}(\text{CH}_4)$, and to estimate its potential impact on the estimation of CH₄ sources and isotopic signatures with top-down approaches.

~~We tested a realistic range of Cl concentrations, i.e., resulting in Cl tropospheric and stratospheric oxidations that are in agreement with recently published studies. We also included a Cl field suggested by the GCP 2018 protocol to be prescribed in inverse simulations in order to investigate its influence on and values in comparison with more realistic and recent Cl fields. The realistic~~ The Cl fields tested here are responsible for between 0.3 % and ~~1.88~~ 1.5 % of the total CH₄ sink in the troposphere and between 1.0 % and ~~1.21~~ 1.6 % in the stratosphere.

~~At the surface, the change in the Cl field and thus in the associated sink results in a bias in~~ The differences in prescribed Cl
670 concentrations lead to biases in simulated CH₄ mole fractions ~~that reaches a maximum value of 44.5 at steady state. An and~~ $\delta^{13}\text{C}(\text{CH}_4)$ isotopic composition that increase over time but stabilize after several decades.

We develop three methods to predict how an inversion system would adjust the surface fluxes by a value of 12.3 global emissions and source signatures in order to compensate for these biases. This adjustment-CH₄ and δ¹³C(CH₄) biases. The most robust method (M1) provides flux adjustments ranging from -7.0 (no Cl sink) to +46.8 TgCH₄.yr⁻¹ (Cl-Taki). The two other methods yield similar ranges. We show that these adjustment values linearly depend on tropospheric Cl concentrations and that each increase by 1000 molec.cm⁻³ in the mean tropospheric Cl concentration would require an adjustment of +11.7 TgCH₄.yr⁻¹. However, most of the fields tested here lead to an adjustment below 10 TgCH₄.yr⁻¹. It therefore remains small in comparison to the uncertainties inferred by Saunois et al. (2020). However, the use of perhaps more unrealistic Cl fields (as suggested by recent literature) can generate much larger biases.

values at the surface are also shifted by a change in the prescribed Cl field. In particular, we find an increase in the global mean at the surface of 0.53‰. The same method is applied to quantify the globally-averaged globally-averaged δ¹³C(CH₄)_{source} adjustment. We also find a good linear relationship between the adjustment and the mean tropospheric Cl concentration. A source signature adjustment of -1.0‰ at the surface for each additional percent of contribution from the tropospheric Cl sink to the total sink. In an inversion, this additional percent of contribution would reduce the inferred would therefore result from an increase of 1000 molec.cm⁻³ in the mean tropospheric Cl concentration to compensate for the enhanced atmospheric isotopic fractionation. After discarding the Cl-Taki field and the possibility of neglecting the Cl sink, we estimate that the globally-averaged isotopic signature by 0.53‰ source signature ranges from -53.1 to -52.2‰. This range represents the uncertainty in globally-averaged source signature resulting from uncertainties in tropospheric Cl concentrations. However, it does not account for other uncertainties, e.g., those related to the KIE of the OH sink. Also, we find that intrusions of stratospheric air are responsible for an enrichment of δ¹³C(CH₄) by 0.30‰ at the surface between 1998 and 2018. Neglecting the influence of stratospheric Cl on in comparison with an atmosphere without stratospheric Cl. We also show here that the choice of the Cl field has a very strong influence on the source mixture obtained with an inversion assimilating δ¹³C(CH₄) surface values could therefore increase the global mean isotopic signature estimated by an inversion by 0.30 observations.

seasonal cycles are only slightly influenced by a A modification of the Cl sink (1-2% change in the seasonal cycle amplitude). Changing the Cl field field within the tested range only slightly influences CH₄ seasonal cycles. It can nevertheless modify the amplitudes of δ¹³C(CH₄) seasonal cycle by up to 10-20% for most of the tested fields, depending on the latitude. To compensate for this change in seasonal cycles, an inversion system might reduce or amplify the seasonal cycles of each emission categories, in particular those which have a large impact on the δ¹³C(CH₄) seasonal cycle, namely wetlands and biomass burning.

We also investigate the influence of Cl concentrations on the modeling of CH₄ and δ¹³C(CH₄) vertical profiles. We find that stratospheric model-observation Observed profiles are well captured by the model, although simulated CH₄ mole fractions are generally larger than observed values above the tropopause. We conclude that these discrepancies in LMDz-SACS are unlikely to be caused by a misrepresentation of the Cl sink, although a change in Cl concentrations can shift mole fractions at 25 km by up to 130. Also, a change in the tropospheric Cl sink influences tropospheric and stratospheric mole fractions to the same magnitude.

~

It is difficult to conclude which CI field provides the most realistic representation of the CI sink among those tested here. Recent developments and efforts have nevertheless narrowed the range of uncertainties regarding the CI concentrations (less than 1.1×10^3 molec.cm⁻³ in the troposphere and $1.4\text{-}1.6 \times 10^5$ molec.cm⁻³ in the stratosphere). Our study shows that the impact of a change in CI field on top-down CH₄ flux estimates should be small compared to current uncertainties in Saunois et al. (2020) if this change is made within ~~a realistic the~~ range of CI concentrations ~~both in the troposphere and the stratosphere recently estimated~~. A CI ~~configuration distribution~~ for all inversions agreed upon in multi-model studies such as Saunois et al. (2020) should ~~however~~ reduce the spread in estimated CH₄ ~~emission~~ fluxes. We ~~show that the choice of the CI field is however critical (both in the troposphere and the stratosphere) for the global estimates of an inversion assimilating observations and can lead to radically different source mixtures and/or source signatures~~ suggest to adopt recent estimates, especially that of Wang et al. (2021) which results from the most comprehensive study to date.

Data availability. The data for CH₄ and $\delta^{13}\text{C}(\text{CH}_4)$ observations were downloaded from the NOAA-ESRL server https://www.esrl.noaa.gov/gmd/aftp/data/trace_gases. Datasets for the input emissions were provided by the Global Carbon Project (GCP) team. The AirCore vertical profiles from the NOAA-ESRL Aircraft Program (DOI: 10.15138/6AV0-MY81, Version: 20181101) were provided by CS and BB. The CI-Sherwen and CI-Wang fields were provided by the corresponding authors of Sherwen et al. (2016b) and Wang et al. (2021), respectively. The CI-INCA field, the modeling output files and the AirCore vertical profiles from the French AirCore Program are available upon request from the corresponding author.

Author contributions. JT designed and run the simulation experiments and performed the data analysis presented in this paper. DH provided the CI-INCA field used for the simulations. MS provided the CH₄ fluxes. CS and BB provided the AirCore vertical profiles from the NOAA-ESRL Aircraft Program. MS, AB, IP and PB provided scientific, technical expertise and contributed to the scientific analysis of this work. JT prepared the manuscript with contributions from all co-authors.

Competing interests. The authors declare that they have no conflict of interest.

Acknowledgements. This work was supported by the CEA (Commissariat à l'Énergie Atomique et aux Énergies Alternatives). The study extensively relies on the meteorological data provided by the ECMWF. Calculations were performed using the computing resources of LSCE, maintained by François Marabelle and the LSCE IT team. The authors wish to thank the measurement teams from the NOAA GML and from INSTAAR for their work. Finally, the authors thank the three referees for their fruitful comments and suggestions on our manuscript.

References

- Allan, W., Struthers, H., and Lowe, D. C.: Methane carbon isotope effects caused by atomic chlorine in the marine boundary layer: Global model results compared with Southern Hemisphere measurements, *Journal of Geophysical Research*, 112, <https://doi.org/10.1029/2006JD007369>, 2007.
- Baier, B., Sweeney, C., T., N., Higgs, J., Wolter, S., and Laboratory, N. G. M.: NOAA AirCore atmospheric sampling system profiles (Version 20181101) [Data set], NOAA GML, <https://doi.org/10.15138/6AV0-MY81>, 2021.
- Bousquet, P., Ciais, P., Miller, J. B., Dlugokencky, E. J., Hauglustaine, D. A., Prigent, C., Van der Werf, G. R., Peylin, P., Brunke, E.-G., Carouge, C., Langenfelds, R. L., Lathière, J., Papa, F., Ramonet, M., Schmidt, M., Steele, L. P., Tyler, S. C., and White, J.: Contribution of anthropogenic and natural sources to atmospheric methane variability, *Nature*, 443, 439–443, <https://doi.org/10.1038/nature05132>, 2006.
- Burkholder, J. B., Abbatt, J. P. D., Huie, R. E., Kurylo, M. J., Wilmouth, D. M., Sander, S. P., Barker, J. R., Kolb, C. E., Orkin, V. L., and Wine, P. H.: JPL Publication 15-10: Chemical Kinetics and Photochemical Data for Use in Atmospheric Studies, p. 1392, 2015.
- Butchart, N.: The Brewer-Dobson circulation, *Reviews of Geophysics*, 52, 157–184, <https://doi.org/10.1002/2013RG000448>, [_eprint: https://onlinelibrary.wiley.com/doi/pdf/10.1002/2013RG000448](https://onlinelibrary.wiley.com/doi/pdf/10.1002/2013RG000448), 2014.
- Cantrell, C. A., Shetter, R. E., McDaniel, A. H., Calvert, J. G., Davidson, J. A., Lowe, D. C., Tyler, S. C., Cicerone, R. J., and Greenberg, J. P.: Carbon kinetic isotope effect in the oxidation of methane by the hydroxyl radical, *Journal of Geophysical Research: Atmospheres*, 95, 22 455–22 462, <https://doi.org/doi.org/10.1029/JD095iD13p22455>, 1990.
- Chevallier, F., Fisher, M., Peylin, P., Serrar, S., Bousquet, P., Bréon, F.-M., Chédin, A., and Ciais, P.: Inferring CO₂ sources and sinks from satellite observations: Method and application to TOVS data, *Journal of Geophysical Research*, 110, <https://doi.org/10.1029/2005JD006390>, 2005.
- Craig, H.: Isotopic standards for carbon and oxygen and correction factors for mass-spectrometric analysis of carbon dioxide, *Geochimica et Cosmochimica Acta*, 12, 133–149, [https://doi.org/10.1016/0016-7037\(57\)90024-8](https://doi.org/10.1016/0016-7037(57)90024-8), 1957.
- Dlugokencky, E. J.: NOAA/GML, www.esrl.noaa.gov/gmd/ccgg/trends_ch4/, last access : 12 July 2021, 2021.
- Dlugokencky, E. J.: NOAA/GML, www.esrl.noaa.gov/gmd/ccgg/trends_ch4/, last access : 9 May 2022, 2022.
- Etheridge, D. M., Steele, L. P., Francey, R. J., and Langenfelds, R. L.: Atmospheric methane between 1000 A.D. and present: Evidence of anthropogenic emissions and climatic variability, *Journal of Geophysical Research: Atmospheres*, 103, 15 979–15 993, <https://doi.org/10.1029/98JD00923>, 1998.
- Fletcher, S. E. M., Tans, P. P., Bruhwiler, L. M., Miller, J. B., and Heimann, M.: CH₄ sources estimated from atmospheric observations of CH₄ and its ¹³C/¹²C isotopic ratios: 2. Inverse modeling of CH₄ fluxes from geographical regions, *Global Biogeochemical Cycles*, 18, <https://doi.org/10.1029/2004GB002224>, 2004.
- Folberth, G. A., Hauglustaine, D. A., Lathière, J., and Brocheton, F.: Interactive chemistry in the Laboratoire de Météorologie Dynamique general circulation model: model description and impact analysis of biogenic hydrocarbons on tropospheric chemistry, *Atmospheric Chemistry and Physics*, 6, 2273–2319, <https://doi.org/10.5194/acp-6-2273-2006>, 2006.
- Fujita, R., Morimoto, S., Maksyutov, S., Kim, H.-S., Arshinov, M., Brailsford, G., Aoki, S., and Nakazawa, T.: Global and Regional CH₄ Emissions for 1995–2013 Derived From Atmospheric CH₄, δ¹³C-CH₄, and δD-CH₄ Observations and a Chemical Transport Model, *Journal of Geophysical Research: Atmospheres*, 125, e2020JD032 903, <https://doi.org/doi.org/10.1029/2020JD032903>, 2020.

- Ganesan, A. L., Stell, A. C., Gedney, N., Comyn-Platt, E., Hayman, G., Rigby, M., Poulter, B., and Hornibrook, E. R. C.: Spatially Resolved Isotopic Source Signatures of Wetland Methane Emissions, *Geophysical Research Letters*, 45, 3737–3745, <https://doi.org/10.1002/2018GL077536>, 2018.
- 770 Gromov, S., Brenninkmeijer, C. A. M., and Jöckel, P.: A very limited role of tropospheric chlorine as a sink of the greenhouse gas methane, *Atmospheric Chemistry and Physics*, 18, 9831–9843, <https://doi.org/doi.org/10.5194/acp-18-9831-2018>, 2018.
- Gupta, M., Tyler, S., and Cicerone, R.: Modeling atmospheric $\delta^{13}\text{C}\text{H}_4$ and the causes of recent changes in atmospheric CH_4 amounts, *Journal of Geophysical Research: Atmospheres*, 101, 22 923–22 932, <https://doi.org/10.1029/96JD02386>, 1996.
- Hauglustaine, D. A., Hourdin, F., Jourdain, L., Filiberti, M.-A., Walters, S., Lamarque, J.-F., and Holland, E. A.: Interactive chemistry in
775 the Laboratoire de Météorologie Dynamique general circulation model: Description and background tropospheric chemistry evaluation, *Journal of Geophysical Research: Atmospheres*, 109, <https://doi.org/10.1029/2003JD003957>, 2004.
- Hauglustaine, D. A., Cozic, A., Caubel, A., Lathière, J., Sépulchre, P., Cohen, Y., Balkanski, Y., Lurton, T., Boucher, O., and Tsigaridis, K.: Coupled Climate-Chemistry-Aerosol simulations under the AerChemMIP scenarios with the IPSL-CM5A2-INCA climate model, in preparation, 2021.
- 780 Hossaini, R., Chipperfield, M. P., Saiz-Lopez, A., Fernandez, R., Monks, S., Feng, W., Brauer, P., and von Glasow, R.: A global model of tropospheric chlorine chemistry: Organic versus inorganic sources and impact on methane oxidation, *Journal of Geophysical Research: Atmospheres*, 121, 14,271–14,297, <https://doi.org/10.1002/2016JD025756>, 2016.
- Hourdin, F., Musat, I., Bony, S., Braconnot, P., Codron, F., Dufresne, J.-L., Fairhead, L., Filiberti, M.-A., Friedlingstein, P., Grandpeix, J.-Y., Krinner, G., LeVan, P., Li, Z.-X., and Lott, F.: The LMDZ4 general circulation model: climate performance and sensitivity to parametrized
785 physics with emphasis on tropical convection, *Climate Dynamics*, 27, 787–813, <https://doi.org/10.1007/s00382-006-0158-0>, 2006.
- Houweling, S., Bergamaschi, P., Chevallier, F., Heimann, M., Kaminski, T., Krol, M., Michalak, A. M., and Patra, P.: Global inverse modeling of CH_4 sources and sinks: an overview of methods, *Atmospheric Chemistry and Physics*, 17, 235–256, <https://doi.org/doi.org/10.5194/acp-17-235-2017>, 2017.
- Karion, A., Sweeney, C., Tans, P., and Newberger, T.: AirCore: An Innovative Atmospheric Sampling System, *Journal of Atmospheric and
790 Oceanic Technology*, 27, 1839–1853, <https://doi.org/10.1175/2010JTECHA1448.1>, 2010.
- Lassey, K. R., Lowe, D. C., and Manning, M. R.: The trend in atmospheric methane $\delta^{13}\text{C}$ and implications for isotopic constraints on the global methane budget, *Global Biogeochemical Cycles*, 14, 41–49, <https://doi.org/10.1029/1999GB900094>, 2000.
- Locatelli, R., Bousquet, P., Hourdin, F., Saunio, M., Cozic, A., Couvreux, F., Grandpeix, J.-Y., Lefebvre, M.-P., Rio, C., Bergamaschi, P., Chambers, S. D., Karstens, U., Kazan, V., van der Laan, S., Meijer, H. A. J., Moncrieff, J., Ramonet, M., Scheeren, H. A., Schlosser,
795 C., Schmidt, M., Vermeulen, A., and Williams, A. G.: Atmospheric transport and chemistry of trace gases in LMDz5B: evaluation and implications for inverse modelling, *Geoscientific Model Development*, 8, 129–150, <https://doi.org/10.5194/gmd-8-129-2015>, 2015.
- Louis, J.-F.: A parametric model of vertical eddy fluxes in the atmosphere, *Boundary-Layer Meteorology*, 17, 187–202, <https://doi.org/10.1007/BF00117978>, 1979.
- Mailler, S., Menut, L., Khvorostyanov, D., Valari, M., Couvidat, F., Siour, G., Turquety, S., Briant, R., Tuccella, P., Bessagnet, B., Colette,
800 A., Létinois, L., Markakis, K., and Meleux, F.: CHIMERE-2017: from urban to hemispheric chemistry-transport modeling, *Geoscientific Model Development*, 10, 2397–2423, <https://doi.org/10.5194/gmd-10-2397-2017>, 2017.
- McCarthy, M. C., Connell, P., and Boering, K. A.: Isotopic fractionation of methane in the stratosphere and its effect on free tropospheric isotopic compositions, *Geophysical Research Letters*, 28, 3657–3660, <https://doi.org/10.1029/2001GL013159>, 2001.

- 805 McCarthy, M. C., Boering, K. A., Rice, A. L., Tyler, S. C., Connell, P., and Atlas, E.: Carbon and hydrogen isotopic compositions of stratospheric methane: 2. Two-dimensional model results and implications for kinetic isotope effects, *Journal of Geophysical Research: Atmospheres*, 108, <https://doi.org/10.1029/2002JD003183>, 2003.
- McNorton, J., Wilson, C., Gloor, M., Parker, R. J., Boesch, H., Feng, W., Hossaini, R., and Chipperfield, M. P.: Attribution of recent increases in atmospheric methane through 3-D inverse modelling, *Atmospheric Chemistry and Physics*, 18, 18 149–18 168, <https://doi.org/doi.org/10.5194/acp-18-18149-2018>, 2018.
- 810 Meinshausen, M., Vogel, E., Nauels, A., Lorbacher, K., Meinshausen, N., Etheridge, D. M., Fraser, P. J., Montzka, S. A., Rayner, P. J., Trudinger, C. M., Krummel, P. B., Beyerle, U., Canadell, J. G., Daniel, J. S., Enting, I. G., Law, R. M., Lunder, C. R., O’Doherty, S., Prinn, R. G., Reimann, S., Rubino, M., Velders, G. J. M., Vollmer, M. K., Wang, R. H. J., and Weiss, R.: Historical greenhouse gas concentrations for climate modelling (CMIP6), *Geoscientific Model Development*, 10, 2057–2116, <https://doi.org/doi.org/10.5194/gmd-10-2057-2017>, 2017.
- 815 Membrive, O., Crevoisier, C., Sweeney, C., Danis, F., Hertzog, A., Engel, A., Bönisch, H., and Picon, L.: AirCore-HR: a high-resolution column sampling to enhance the vertical description of CH₄ and CO₂, *Atmos. Meas. Tech.*, p. 20, 2017.
- Menut, L., Bessagnet, B., Khvorostyanov, D., Beekmann, M., Blond, N., Colette, A., Coll, I., Curci, G., Foret, G., Hodzic, A., Mailler, S., Meleux, F., Monge, J.-L., Pison, I., Siour, G., Turquety, S., Valari, M., Vautard, R., and Vivanco, M. G.: CHIMERE 2013: a model for regional atmospheric composition modelling, *Geoscientific Model Development*, 6, 981–1028, <https://doi.org/10.5194/gmd-6-981-2013>,
820 2013.
- Monteil, G., Houweling, S., Dlugokenky, E. J., Maenhout, G., Vaughn, B. H., White, J. W. C., and Rockmann, T.: Interpreting methane variations in the past two decades using measurements of CH₄ mixing ratio and isotopic composition, *Atmospheric Chemistry and Physics*, 11, 9141–9153, <https://doi.org/doi.org/10.5194/acp-11-9141-2011>, 2011.
- Müller, R., Brenninkmeijer, C. A. M., and Crutzen, P. J.: A large ¹³C deficit in the lower Antarctic stratosphere due to “ozone hole” chemistry: Part II, Modeling, *Geophysical Research Letters*, 23, 2129–2132, <https://doi.org/10.1029/96GL01472>, 1996.
- 825 Neef, L., Weele, M. v., and Velthoven, P. v.: Optimal estimation of the present-day global methane budget, *Global Biogeochemical Cycles*, 24, <https://doi.org/10.1029/2009GB003661>, 2010.
- Nisbet, E. G., Manning, M. R., Dlugokenky, E. J., Fisher, R. E., Lowry, D., Michel, S. E., Myhre, C. L., Platt, S. M., Allen, G., Bousquet, P., Brownlow, R., Cain, M., France, J. L., Hermansen, O., Hossaini, R., Jones, A. E., Levin, I., Manning, A. C., Myhre, G., Pyle, J. A.,
830 Vaughn, B. H., Warwick, N. J., and White, J. W. C.: Very Strong Atmospheric Methane Growth in the 4 Years 2014–2017: Implications for the Paris Agreement, *Global Biogeochemical Cycles*, 33, 318–342, <https://doi.org/10.1029/2018GB006009>, 2019.
- Ostler, A., Sussmann, R., Patra, P. K., Houweling, S., Bruine, M. D., Stiller, G. P., Haedel, F. J., Plieninger, J., Bousquet, P., Yin, Y., Saunio, M., Walker, K. A., Deutscher, N. M., Griffith, D. W. T., Blumenstock, T., Hase, F., Warneke, T., Wang, Z., Kivi, R., and Robinson, J.: Evaluation of column-averaged methane in models and TCCON with a focus on the stratosphere, *Atmospheric Measurement Techniques*,
835 9, 4843–4859, <https://doi.org/doi.org/10.5194/amt-9-4843-2016>, 2016.
- Patra, P. K., Houweling, S., Krol, M., Bousquet, P., Belikov, D., Bergmann, D., Bian, H., Cameron-Smith, P., Chipperfield, M. P., Corbin, K., Fortems-Cheiney, A., Fraser, A., Gloor, E., Hess, P., Ito, A., Kawa, S. R., Law, R. M., Loh, Z., Maksyutov, S., Meng, L., Palmer, P. I., Prinn, R. G., Rigby, M., Saito, R., and Wilson, C.: TransCom model simulations of CH₄ and related species: linking transport, surface flux and chemical loss with CH₄ variability in the troposphere and lower stratosphere, *Atmospheric Chemistry and Physics*, 11, 12 813–12 837,
840 <https://doi.org/10.5194/acp-11-12813-2011>, 2011.

- Pison, I., Bousquet, P., Chevallier, F., Szopa, S., and Hauglustaine, D.: Multi-species inversion of CH₄, CO and H₂ emissions from surface measurements, *Atmos. Chem. Phys.*, p. 17, 2009.
- Rice, A. L., Tyler, S. C., McCarthy, M. C., Boering, K. A., and Atlas, E.: Carbon and hydrogen isotopic compositions of stratospheric methane: 1. High-precision observations from the NASA ER-2 aircraft, *Journal of Geophysical Research: Atmospheres*, 108, <https://doi.org/10.1029/2002JD003042>, 2003.
- Rice, A. L., Butenhoff, C. L., Teama, D. G., Röger, F. H., Khalil, M. A. K., and Rasmussen, R. A.: Atmospheric methane isotopic record favors fossil sources flat in 1980s and 1990s with recent increase, *Proceedings of the National Academy of Sciences*, 113, 10 791–10 796, <https://doi.org/10.1073/pnas.1522923113>, 2016.
- Rigby, M., Manning, A. J., and Prinn, R. G.: The value of high-frequency, high-precision methane isotopologue measurements for source and sink estimation, *Journal of Geophysical Research: Atmospheres*, 117, <https://doi.org/10.1029/2011JD017384>, 2012.
- Röckmann, T., Groöß, J.-U., and Müller, R.: The impact of anthropogenic chlorine emissions, stratospheric ozone change and chemical feedbacks on stratospheric water, *Atmospheric Chemistry and Physics*, 4, 693–699, <https://doi.org/10.5194/acp-4-693-2004>, 2004.
- Röckmann, T., Brass, M., Borchers, R., and Engel, A.: The isotopic composition of methane in the stratosphere: high-altitude balloon sample measurements, *Atmospheric Chemistry and Physics*, 11, 13 287–13 304, <https://doi.org/10.5194/acp-11-13287-2011>, 2011.
- Saueressig, G., Bergamaschi, P., Crowley, J. N., Fischer, H., and Harris, G. W.: Carbon kinetic isotope effect in the reaction of CH₄ with Cl atoms, *Geophysical Research Letters*, 22, 1225–1228, <https://doi.org/10.1029/95GL00881>, 1995.
- Saueressig, G., Crowley, J. N., Bergamaschi, P., Brühl, C., Brenninkmeijer, C. A. M., and Fischer, H.: Carbon 13 and D kinetic isotope effects in the reactions of CH₄ with O(¹D) and OH: New laboratory measurements and their implications for the isotopic composition of stratospheric methane, *Journal of Geophysical Research: Atmospheres*, 106, 23 127–23 138, <https://doi.org/10.1029/2000JD000120>, 2001.
- Saunois, M., Stavert, A. R., Poulter, B., Bousquet, P., Canadell, J. G., Jackson, R. B., Raymond, P. A., Dlugokencky, E. J., Houweling, S., Patra, P. K., Ciais, P., Arora, V. K., Bastviken, D., Bergamaschi, P., Blake, D. R., Brailsford, G., Bruhwiler, L., Carlson, K. M., Carrol, M., Castaldi, S., Chandra, N., Crevoisier, C., Crill, P. M., Covey, K., Curry, C. L., Etiope, G., Frankenberg, C., Gedney, N., Hegglin, M. I., Höglund-Isaksson, L., Hugelius, G., Ishizawa, M., Ito, A., Janssens-Maenhout, G., Jensen, K. M., Joos, F., Kleinen, T., Krummel, P. B., Langenfelds, R. L., Laruelle, G. G., Liu, L., Machida, T., Maksyutov, S., McDonald, K. C., McNorton, J., Miller, P. A., Melton, J. R., Morino, I., Müller, J., Murguía-Flores, F., Naik, V., Niwa, Y., Noce, S., O'Doherty, S., Parker, R. J., Peng, C., Peng, S., Peters, G. P., Prigent, C., Prinn, R., Ramonet, M., Regnier, P., Riley, W. J., Rosentreter, J. A., Segers, A., Simpson, I. J., Shi, H., Smith, S. J., Steele, L. P., Thornton, B. F., Tian, H., Tohjima, Y., Tubiello, F. N., Tsuruta, A., Viovy, N., Voulgarakis, A., Weber, T. S., van Weele, M., van der Werf, G. R., Weiss, R. F., Worthy, D., Wunch, D., Yin, Y., Yoshida, Y., Zhang, W., Zhang, Z., Zhao, Y., Zheng, B., Zhu, Q., Zhu, Q., and Zhuang, Q.: The Global Methane Budget 2000–2017, *Earth System Science Data*, 12, 1561–1623, <https://doi.org/10.5194/essd-12-1561-2020>, 2020.
- Schaefer, H., Fletcher, S. E. M., Veidt, C., Lassey, K. R., Brailsford, G. W., Bromley, T. M., Dlugokencky, E. J., Michel, S. E., Miller, J. B., Levin, I., Lowe, D. C., Martin, R. J., Vaughn, B. H., and White, J. W. C.: A 21st-century shift from fossil-fuel to biogenic methane emissions indicated by ¹³CH₄, *Science*, 352, 80–84, <https://doi.org/10.1126/science.aad2705>, 2016.
- Schwietzke, S., Sherwood, O. A., Bruhwiler, L. M. P., Miller, J. B., Etiope, G., Dlugokencky, E. J., Michel, S. E., Arling, V. A., Vaughn, B. H., White, J. W. C., and Tans, P. P.: Upward revision of global fossil fuel methane emissions based on isotope database, *Nature*, 538, 88–91, <https://doi.org/10.1038/nature19797>, 2016.

- 880 Sherwen, T., Evans, M. J., Carpenter, L. J., Andrews, S. J., Lidster, R. T., Dix, B., Koenig, T. K., Sinreich, R., Ortega, I., Volkamer, R., Saiz-Lopez, A., Prados-Roman, C., Mahajan, A. S., and Ordóñez, C.: Iodine's impact on tropospheric oxidants: a global model study in GEOS-Chem, *Atmospheric Chemistry and Physics*, 16, 1161–1186, <https://doi.org/10.5194/acp-16-1161-2016>, publisher: Copernicus GmbH, 2016a.
- 885 Sherwen, T., Schmidt, J. A., Evans, M. J., Carpenter, L. J., Großmann, K., Eastham, S. D., Jacob, D. J., Dix, B., Koenig, T. K., Sinreich, R., Ortega, I., Volkamer, R., Saiz-Lopez, A., Prados-Roman, C., Mahajan, A. S., and Ordóñez, C.: Global impacts of tropospheric halogens (Cl, Br, I) on oxidants and composition in GEOS-Chem, *Atmospheric Chemistry and Physics*, 16, 12239–12271, <https://doi.org/10.5194/acp-16-12239-2016>, 2016b.
- Sherwood, O. A., Schwietzke, S., Arling, V. A., and Etiope, G.: Global Inventory of Gas Geochemistry Data from Fossil Fuel, Microbial and Burning Sources, version 2017, *Earth System Science Data*, 9, 639–656, <https://doi.org/10.5194/essd-9-639-2017>, 2017.
- Stolper, D. A., Sessions, A. L., Ferreira, A. A., Santos Neto, E. V., Schimmelmann, A., Shusta, S. S., Valentine, D. L., and Eiler, J. M.: Combined ^{13}C -D and D-D clumping in methane: Methods and preliminary results, *Geochimica et Cosmochimica Acta*, 126, 169–191, <https://doi.org/10.1016/j.gca.2013.10.045>, 2014.
- 890 Strode, S. A., Wang, J. S., Manyin, M., Duncan, B., Hossaini, R., Keller, C. A., Michel, S. E., and White, J. W. C.: Strong sensitivity of the isotopic composition of methane to the plausible range of tropospheric chlorine, *Atmospheric Chemistry and Physics*, 20, 8405–8419, <https://doi.org/10.5194/acp-20-8405-2020>, 2020.
- Takigawa, M., Takahashi, M., and Akiyoshi, H.: Simulation of ozone and other chemical species using a Center for Climate System Research/National Institute for Environmental Studies atmospheric GCM with coupled stratospheric chemistry, *Journal of Geophysical Research: Atmospheres*, 104, 14003–14018, <https://doi.org/10.1029/1998JD100105>, 1999.
- 895 Terrenoire, E., Hauglustaine, D., Cohen, Y., Cozic, A., Valorso, R., Lefèvre, F., and Matthes, S.: Impact of present and future aircraft NO_x and aerosol emissions on atmospheric composition and associated direct radiative forcing of climate, *Atmospheric Chemistry and Physics Discussions*, 2022, 1–39, <https://doi.org/10.5194/acp-2022-222>, 2022.
- 900 Thanwerdas, J., Saunois, M., Berchet, A., Pison, I., Vaughn, B. H., Michel, S. E., and Bousquet, P.: Variational inverse modelling within the Community Inversion Framework to assimilate $\delta^{13}\text{C}(\text{CH}_4)$ and CH_4 : a case study with model LMDz-SACS, *Geoscientific Model Development Discussions*, pp. 1–29, <https://doi.org/10.5194/gmd-2021-106>, 2021.
- Thompson, R. L., Nisbet, E. G., Pisso, I., Stohl, A., Blake, D., Dlugokencky, E. J., Helmig, D., and White, J. W. C.: Variability in Atmospheric Methane From Fossil Fuel and Microbial Sources Over the Last Three Decades, *Geophysical Research Letters*, 45, 11,499–11,508, <https://doi.org/10.1029/2018GL078127>, 2018.
- 905 Tiedtke, M.: A Comprehensive Mass Flux Scheme for Cumulus Parameterization in Large-Scale Models, *Monthly Weather Review*, 117, 1779–1800, [https://doi.org/10.1175/1520-0493\(1989\)117<1779:ACMFSF>2.0.CO;2](https://doi.org/10.1175/1520-0493(1989)117<1779:ACMFSF>2.0.CO;2), 1989.
- Wang, J. S., McElroy, M. B., Spivakovsky, C. M., and Jones, D. B. A.: On the contribution of anthropogenic Cl to the increase in $\delta^{13}\text{C}$ of atmospheric methane: ANTHROPOGENIC Cl AND $\delta^{13}\text{C}$ OF METHANE, *Global Biogeochemical Cycles*, 16, 20–1–20–11, <https://doi.org/10.1029/2001GB001572>, 2002.
- 910 Wang, X., Jacob, D. J., Eastham, S. D., Sulprizio, M. P., Zhu, L., Chen, Q., Alexander, B., Sherwen, T., Evans, M. J., Lee, B. H., Haskins, J. D., Lopez-Hilfiker, F. D., Thornton, J. A., Huey, G. L., and Liao, H.: The role of chlorine in global tropospheric chemistry, *Atmospheric Chemistry and Physics*, 19, 3981–4003, <https://doi.org/10.5194/acp-19-3981-2019>, 2019.

- 915 Wang, X., Jacob, D. J., Fu, X., Wang, T., Breton, M. L., Hallquist, M., Liu, Z., McDuffie, E. E., and Liao, H.: Effects of Anthropogenic Chlorine on PM_{2.5} and Ozone Air Quality in China, *Environmental Science & Technology*, 54, 9908–9916, <https://doi.org/10.1021/acs.est.0c02296>, 2020.
- 920 Wang, X., Jacob, D. J., Downs, W., Zhai, S., Zhu, L., Shah, V., Holmes, C. D., Sherwen, T., Alexander, B., Evans, M. J., Eastham, S. D., Neuman, J. A., Veres, P., Koenig, T. K., Volkamer, R., Huey, L. G., Bannan, T. J., Percival, C. J., Lee, B. H., and Thornton, J. A.: Global tropospheric halogen (Cl, Br, I) chemistry and its impact on oxidants, *Atmospheric Chemistry and Physics Discussions*, pp. 1–34, <https://doi.org/10.5194/acp-2021-441>, 2021.
- Warwick, N. J., Cain, M. L., Fisher, R., France, J. L., Lowry, D., Michel, S. E., Nisbet, E. G., Vaughn, B. H., White, J. W. C., and Pyle, J. A.: Using $\delta^{13}\text{C}\text{-CH}_4$ and $\delta\text{D}\text{-CH}_4$ to constrain Arctic methane emissions, *Atmospheric Chemistry and Physics*, 16, 14 891–14 908, <https://doi.org/10.5194/acp-16-14891-2016>, 2016.
- 925 White, J. W. C., Vaughn, B. H., and Michel, S. E.: Stable isotopic composition of atmospheric methane (^{13}C) from the NOAA ESRL Carbon Cycle Cooperative Global Air Sampling Network, 1998–2018, available at ftp://aftp.cmdl.noaa.gov/data/trace_gases/ch4c13/flask/, last access: 12 July 2021, 2021.
- 930 Zhao, Y., Saunio, M., Bousquet, P., Lin, X., Berchet, A., Hegglin, M. I., Canadell, J. G., Jackson, R. B., Hauglustaine, D. A., Szopa, S., Stavert, A. R., Abraham, N. L., Archibald, A. T., Bekki, S., Deushi, M., Jöckel, P., Josse, B., Kinnison, D., Kirner, O., Marécal, V., O’Connor, F. M., Plummer, D. A., Revell, L. E., Rozanov, E., Stenke, A., Strode, S., Tilmes, S., Dlugokencky, E. J., and Zheng, B.: Inter-model comparison of global hydroxyl radical (OH) distributions and their impact on atmospheric methane over the 2000–2016 period, *Atmospheric Chemistry and Physics*, 19, 13 701–13 723, <https://doi.org/10.5194/acp-19-13701-2019>, 2019.
- Zhao, Y., Saunio, M., Bousquet, P., Lin, X., Berchet, A., Hegglin, M. I., Canadell, J. G., Jackson, R. B., Dlugokencky, E. J., Langenfelds, R. L., Ramonet, M., Worthy, D., and Zheng, B.: Influences of hydroxyl radicals (OH) on top-down estimates of the global and regional methane budgets, *Atmospheric Chemistry and Physics*, 20, 9525–9546, <https://doi.org/doi.org/10.5194/acp-20-9525-2020>, 2020.

and biases averaged over bands of latitude. Solid lines are the monthly simulated values and dashed lines are the extended values following the methods from Sect. ??.

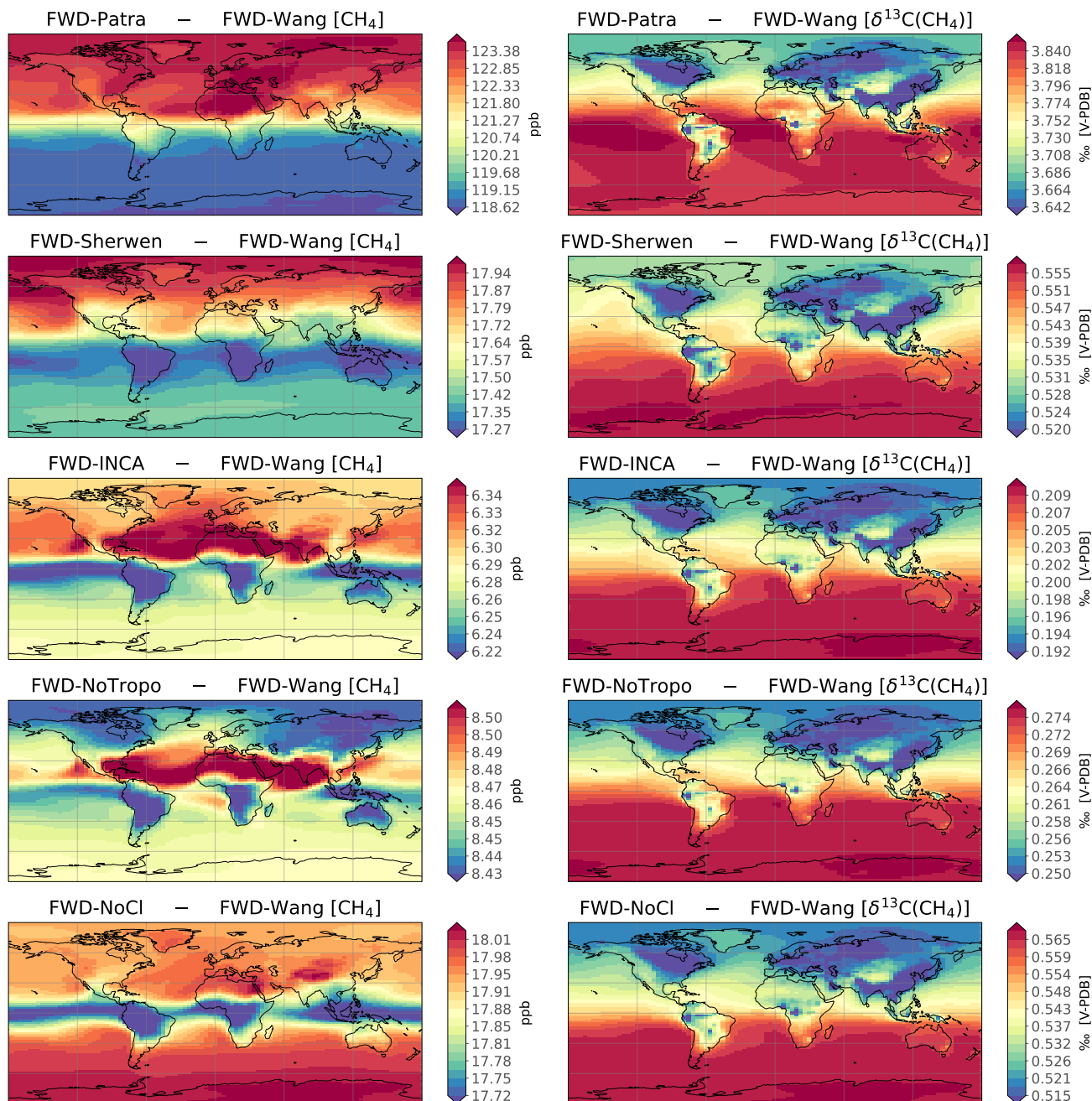


Figure 2. Surface absolute bias between FWD-* and FWD-Wang simulations averaged over 2010-2018. Temporal average is performed before subtraction. First column displays the biases between CH₄ mole fractions. Second column shows the biases between $\delta^{13}\text{C}(\text{CH}_4)$ values. Note that the scales are different for each panel.

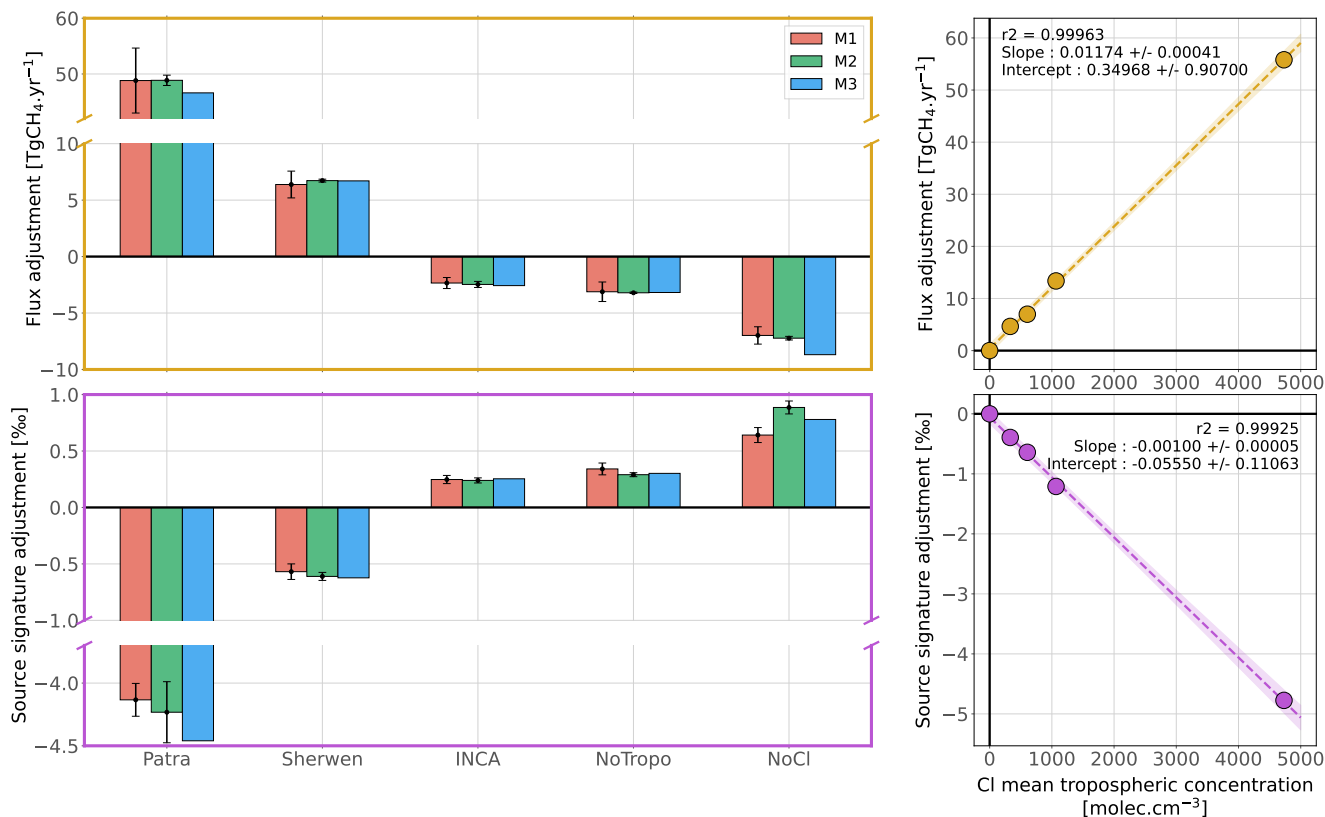


Figure 3. Global CH₄ flux and $\delta^{13}\text{C}(\text{CH}_4)_{\text{source}}$ source signature adjustment due to a change in the prescribed Cl field. Left panels show the adjustments for global CH₄ flux (upper panel) and $\delta^{13}\text{C}(\text{CH}_4)_{\text{source}}$ source signature (lower panel), with multiple methods (M1, M2 and M3) presented in Sect. 2.5 and supplementary Text S1, S2 and S3. Simulations with Cl-Wang are taken as a reference. For M1 and M2, the error bars correspond to the inter-annual variations (one standard deviation) of adjustments. Right panels display the linear model derived from the relationship between the adjustments (estimated with M1) and the mean tropospheric concentration of the prescribed Cl fields. For the linear regression only, simulations without the Cl sink (NoCl) are taken as a reference to calculate the adjustments.

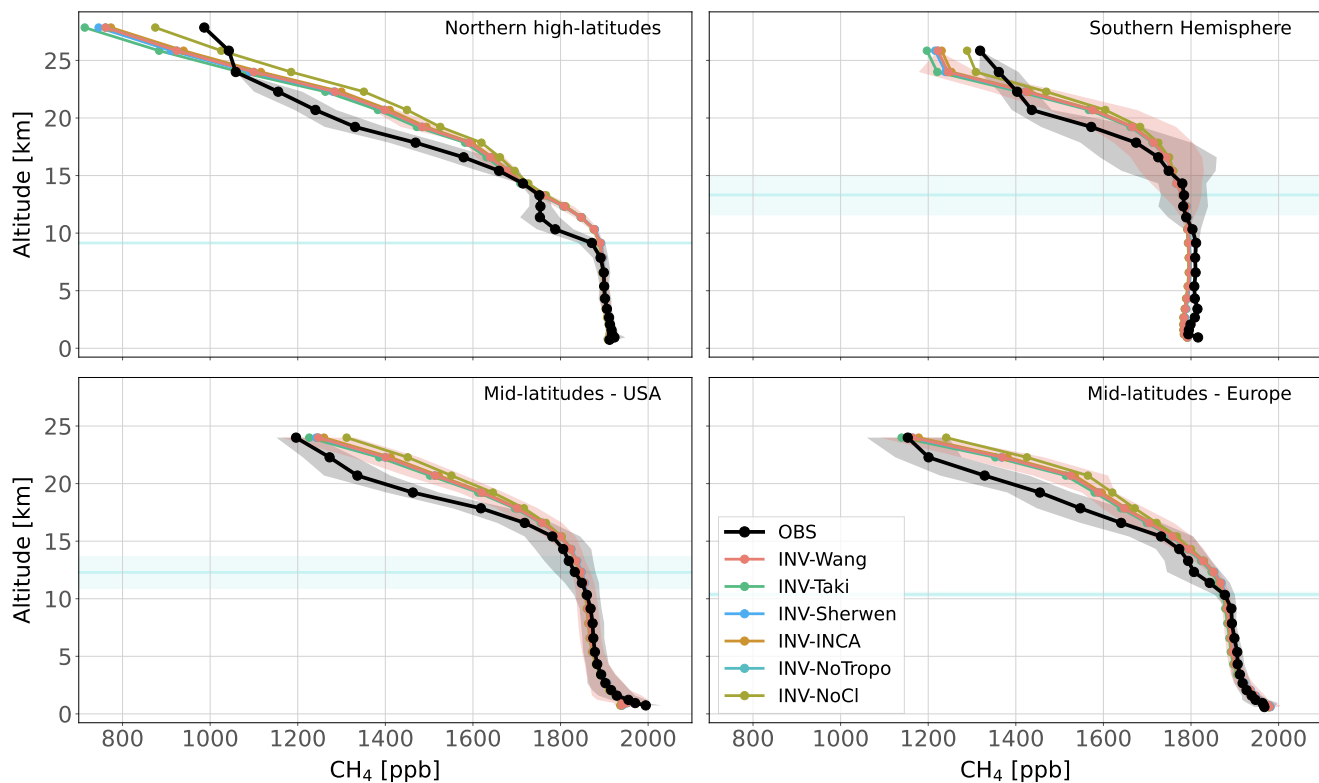


Figure 4. Observed and simulated CH₄ vertical profiles for four regions. All available vertical profiles in each region have been averaged. Shaded areas indicate the standard deviations of this average. Blue line and its associated shaded area show the mean altitude of the tropopause and its standard deviation over the vertical profiles in the region.

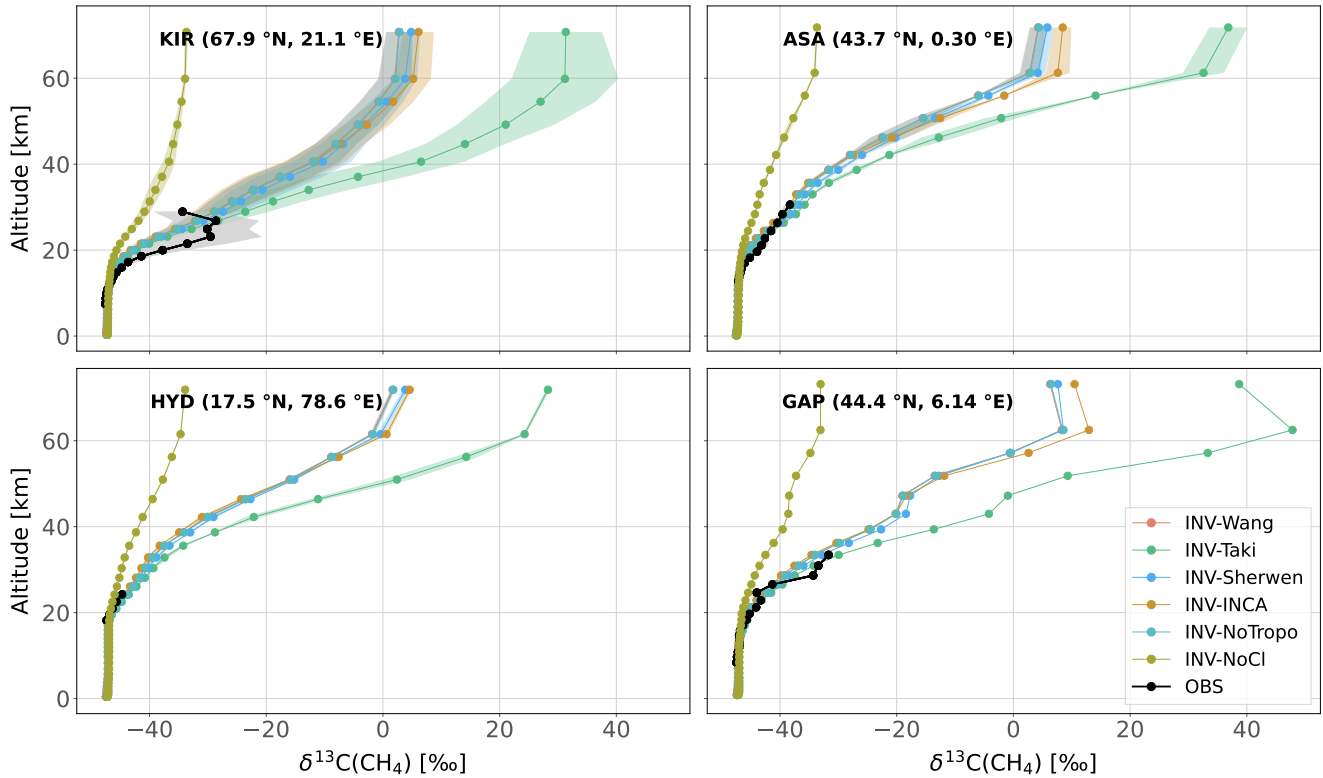


Figure 5. Observed and simulated $\delta^{13}\text{C}(\text{CH}_4)$ vertical profiles for **the Northern Hemisphere (left panel) and Southern Hemisphere (right panel) four locations**. All available vertical profiles in each region have been averaged. Shaded areas indicate the standard deviations of this average. Note that measurement uncertainties (around 0.2 ‰) are much lower than the x-axis range. KIR : Kiruna, Sweden (67.9 °N, 21.10 °E) ; ASA : Aire sur l'Adour, France (43.70 °N, 0.30 °E) ; HYD : Hyderabad, India (17.5 °N, 78.60 °E) ; GAP : Gap, France (44.44 °N, 6.14 °E).